npj | microgravity

Article

Published in cooperation with the Biodesign Institute at Arizona State University, with the support of NASA

https://doi.org/10.1038/s41526-025-00510-y

BMP9 attenuates microgravity-related disuse osteoporosis by modulating TGFβ and BMP signaling

Haoyang Zhao[1,2,3], Mengfan Yang[1,3], Yujiao Liu[1], Xiaolin Tu[1,2] ✉ & Gaohai Shao[1] ✉

Disuse osteoporosis, caused by mechanical unloading, is linked to dysregulated TGFβ and BMP signaling. This study explores their roles and evaluates BMP9 as a potential therapy. A hindlimb unloading (HLU) mouse model was used to assess bone changes and signaling alterations. In vitro, a Rotary Cell Culture System (RCCS) with 3D printing simulated microgravity. BMP9 was overexpressed in bone marrow stromal cells (BMSCs) and osteocytes treated with TGFβ1. HLU mice showed reduced bone density, microstructural integrity, and dysregulated signaling (increased p-Smad2/3, decreased p-Smad1/5/8). BMP9 overexpression restored osteogenic differentiation in vitro and improved bone properties in vivo. However, RCCS failed to replicate osteogenic inhibition, likely due to shear stress. Despite challenges, BMP9 shows promise for treating disuse osteoporosis. Future research will refine vector specificity and reduce immunogenicity for clinical application.

Osteoporosis, as a systemic bone metabolism disorder, currently affects approximately 200 million people worldwide[1]. Its hallmark features, such as decreased bone mineral density and microstructural damage, significantly increase the risk of fractures[2]. With the rising global prevalence of osteoporosis, the disease poses a significant public health burden, with direct annual treatment costs for osteoporotic fractures in Canada, Europe, and the United States alone reaching 5 to 6.5 trillion USD—excluding indirect costs such as disability and lost productivity[3,4]. Amid the dual pressures of population aging and healthcare system reforms[5,6], there is an urgent need to explore the diverse mechanisms underlying the development of osteoporosis, with the goal of identifying effective molecular targets and intervention strategies.

Numerous studies have shown that the onset of osteoporosis is closely associated with a variety of factors, including, but not limited to, changes in hormone levels[7–9] and natural aging[10–12]. Specifically, the cellular and molecular mechanisms involved in osteoporosis are still complex; however, with the growing depth of research into bone biology, the elucidation of the molecular mechanisms governing the communication and coordination networks between osteoblasts (bone formation), osteoclasts (bone resorption), and osteocytes (resident bone cells in the bone matrix) has led to the identification of multiple targets and therapeutic strategies[13,14]. Disuse osteoporosis is a distinct form of secondary osteoporosis, directly resulting from the loss of mechanical loading on bones, which leads to an imbalance between bone synthesis and resorption[15]. It is commonly observed in patients with extended bed rest secondary to spinal cord injury (SCI) and in astronauts on long-duration space missions[16–20]. Notably, disuse osteoporosis, as a subtype caused by the absence of mechanical stress, shares striking pathological similarities with age-related osteoporosis[21]. This similarity underscores the high scientific and social value of exploring its underlying molecular mechanisms and developing targeted therapeutic strategies.

The Transforming Growth Factor β (TGFβ) signaling family, which includes TGFβs, activins, inhibins, as well as various Bone Morphogenetic Proteins (BMPs) and Growth and Differentiation Factors (GDFs), plays essential roles in all cells and tissues, including soft connective tissues and bone. Specific members of the TGFβ family exert different functions in these tissues, with their activity often balanced with that of other TGFβ family members. They interact with various signaling pathways to regulate multiple cellular processes such as growth, differentiation, migration, and apoptosis[22]. During the development of osteoporosis, the TGFβ signaling family appears to play a critical role, particularly in the determination of mesenchymal stem cell differentiation into fibroblastic, osteoblastic, or adipogenic lineages[23]. Moreover, TGFβ signaling directly or indirectly influences osteoclast development[24]. Additionally, TGFβ signaling in osteocytes has been reported to affect the microstructure and mechanical properties of bone tissue[25,26]. Of particular interest, BMPs, members of the TGFβ family, are known to be directly involved in osteoblast differentiation[27,28], with BMP9 (GDF2) being recognized as the BMP factor with the strongest osteogenic potential[29,30]. This effect is not only evident in its ability to promote successful differentiation of mesenchymal stem cells but also in its insensitivity to endogenous inhibitors like noggin[31]. Therefore, compared to other BMP family members, BMP9's

[1]Department of Orthopedics, Affiliated Yongchuan Hospital of Chongqing Medical University, Chongqing, 402160, China. [2]Key Laboratory of Diagnostic Medicine Designated by the Chinese Ministry of Education, College of Laboratory Medicine, Chongqing Medical University, Chongqing, 400016, China. [3]These authors contributed equally: Haoyang Zhao, Mengfan Yang. ✉e-mail: xiaolintt@hotmail.com; shaogaohai567@hospital.cqmu.edu.cn

unique response to microgravity and its resistance to inhibition make it a promising therapeutic candidate.

Results

Microstructural damage of femurs in the hindlimb unloading group of mice associated with overactivation of p-Smad2/3

Micro-CT analysis of the HLU/Tail-suspension model showed that after two weeks of hindlimb unloading, the average trabecular bone mineral density (Tb.BMD) in the unloading group was more than 30% lower than that of the control group (with normal hindlimb loading). A greater than 10% difference in cortical bone mineral density (Ct.BMD) was also observed between the groups. Additionally, the bone volume percentage (BV/TV) for the hindlimb unloading (HLU) and normal loading (NL) groups was 31% and 19%, respectively. Significant differences in trabecular number (Tb.N) and trabecular thickness (Tb.Th) were also observed ($n = 6$, $p < 0.01$, t-test), indicating degradation of bone tissue microstructure (Fig. 1A,B). Bone morphology analysis showed disruption of the osteoblast-osteoclast balance (Fig. 1C). Furthermore, Alcian Blue-Periodic Acid-Schiff (AB-PAS) staining revealed suppression of chondrogenic differentiation and limited hypertrophy of chondrocytes (Fig. 1C). Additionally, silver nitrate staining demonstrated degradation of the lacunar-canalicular system in the cortical bone of hindlimb unloading (HLU) mice (Fig. 1C, indicated by red arrows), with the presence of empty lacunae potentially accounting for the observed decrease in cortical bone density. Immunohistochemical analysis revealed a marked increase in TGFβ1-positive cells and regions within the bone marrow cavity and cortical bone of hindlimb unloading (HLU) mice, accompanied by a substantial population of p-Smad2/3-positive cells. These findings indicate robust activation of the TGFβ-pSmad2/3 signaling pathway. Conversely, on the trabecular bone surface, levels of p-Smad1/5/8 were modestly reduced in the HLU group compared to the normal loading (NL) group, suggesting potential crosstalk or competition between Smad signaling pathways (Fig. 1D).

The combined use of the RCCS and integrated 3D printing module successfully simulated the molecular phenotype of microgravity in the MLO-Y4 cell line

The combination of the rotating cell culture system and the integrated 3D printer successfully simulated the increased expression of *Sost* in MLO-Y4 cells under microgravity conditions. We also observed elevated expression of osteolytic factors *Mmp3*, *Ctsk*, and *Trap* in MLO-Y4 cells under RCCS-simulated microgravity, suggesting that microgravity may induce osteoclast-mediated bone resorption (Supplementary Fig. 1A, B). Unfortunately, our innovative approach failed to simulate osteogenic inhibition in the osteoblast cell line MC3T3-E1(Supplementary Fig. 1C), chondrocyte cell line ATDC5(Supplementary Fig. 1D), and bone marrow stromal cells (Supplementary Fig. 2A). A simple modeling analysis using differential equations suggested that the main cause may be the high shear stress experienced by the 3D module in liquid (Supplementary Fig. 2C), which does not accurately mimic true microgravity conditions (Supplementary Discussion). Consequently, future experiments will no longer be based on this system.

The Adv-EGFP/BMP9(GDF2) overexpression vector was constructed using the AdMax system for cell and animal experiments

The Adv-EGFP or Adv-BMP9(GDF2) overexpression vectors were constructed by co-transfecting the pBHGlox(delta)E13Cre plasmid with either the pDC316-mCMV-EGFP plasmid or the pDC316-mCMV-EGFP-CMV-BMP9 plasmid into 293 A cells.

In vitro experiments demonstrate that high concentrations of TGFβ1 inhibit osteogenic differentiation of bone marrow stromal cells and may lead to osteocyte-mediated bone resorption

In primary osteocytes, exogenous addition of TGFβ1 increases the levels of phosphorylated Smad2/3 while decreasing the levels of phosphorylated Smad1/5/8 (Fig. 2A). The target genes *Id1/2/3* of the BMP-pSmad1/5/8 signaling pathway are downregulated (Fig. 2B), and the expression of osteolytic factors *Mmp3*, *Ctsk*, and *Trap* increases with the concentration of TGFβ1. Interestingly, after activation of the TGFβ-pSmad2/3 signaling pathway in osteocytes, a resorptive bone environment seems to be actively created, with intracellular pH decreasing, indicating intracellular acidification (Fig. 2C). In the bone marrow stromal cells, exogenous addition of TGFβ1 disrupts the osteogenic environment induced by phosphate and vitamin C. As the concentration of TGFβ1 increases, alkaline phosphatase staining and assays show a decrease in alkaline phosphatase enzyme activity (Fig. 3A, B). Alizarin red staining and relative quantification indicate that the mineralization process is impaired (Fig. 3A, C). The expression of osteogenic genes *Runx2*, *Sp7*, *Alpl*, and *Bsp* is reduced (Fig. 3D). Similarly, we observed a shift in Smad signaling and a reduction in BMP signaling target genes *Id1/2/3* (Fig. 3E, F).

Adv-BMP9 (GDF2) can rescue osteogenic inhibition induced by high concentrations of TGFβ1 and improve the osteocyte-mediated bone resorption environment

Alkaline phosphatase staining and enzyme activity assays show that Adv-BMP9 overexpressing bone marrow stromal cells significantly increase alkaline phosphatase enzyme activity (Fig. 4A, B). Under the characteristic concentration of 10 ng/ml TGFβ1, overexpression of BMP9 (GDF2) in the stromal cell line using Adv-BMP9 led to the recovery of osteogenic genes that were downregulated by high concentrations of TGFβ1, as shown by qPCR (Fig. 4C). Similarly, the BMP-pSmad1/5/8 signaling pathway was restored (Fig. 4D), and the expression of its target genes was also recovered (Fig. 4E). In osteocytes, overexpression of BMP9 (GDF2) restored BMP-pSmad1/5/8 signaling (Fig. 5A, B). Furthermore, it reduced the expression of osteolytic factors *Mmp3*, *Ctsk*, and *Trap* (Fig. 5C, D), and improved the intracellular acid-base balance, thereby reducing the likelihood of osteocyte-mediated bone resorption to some extent.

Adv-BMP9 (GDF2) inhibits osteoclast differentiation and function induced by M-CSF and RANKL

Osteoclast differentiation was induced using mouse bone marrow mononuclear macrophages (BMMs). After infecting the BMMs with Adv-EGFP/Adv-BMP9 (GDF2), M-CSF and RANKL were added to induce osteoclast differentiation for assessment. TRAP-positive cell counting and osteoclast (TRAP-positive, with >3 nuclei) counts showed significant differences between the groups. Adv-BMP9 significantly inhibited osteoclast formation (Fig. 6A, B). Osteoclast differentiation and the expression of marker genes *Nfatc1*, *PU.1*, *c-fos*, *Dcstamp*, *Calcr*, *Trap*, and *Ctsk* were significantly reduced (Fig. 6C). Toluidine blue staining of bovine bone slices showed a significant reduction in osteoclast resorption area (Fig. 6A).

Adv-BMP9 (GDF2) promotes chondrogenic differentiation and inhibits adipogenic differentiation in bone marrow stromal cells

After 7 days of culture under chondrogenic induction medium conditions, Alcian blue staining showed stronger staining in BMP9 (GDF2) overexpressing bone marrow stromal cells, suggesting greater accumulation of glycosaminoglycans and collagen deposition (Fig. 6D). qPCR results also confirmed that overexpression of BMP9 (GDF2) increased the expression of glycosaminoglycans and type II collagen (Fig. 6E). After 7 days of culture under adipogenic induction conditions, Oil Red O staining showed that Adv-BMP9 effectively inhibited intracellular lipid droplet accumulation in bone marrow stromal cells (Fig. 6F). qPCR results also indicated that it indeed inhibited adipogenic differentiation (Fig. 6G).

Adv-BMP9 (GDF2) improves bone loss induced by hindlimb unloading and restores the mechanical properties of the mouse femur

Based on the above results, we hypothesize that Adv-BMP9 can effectively improve disuse osteoporosis. After injecting Adv-BMP9 in the HLU/Tail-suspension model, Micro-CT analysis showed that BMP9 overexpression protected mice from trabecular and cortical bone loss induced by tail

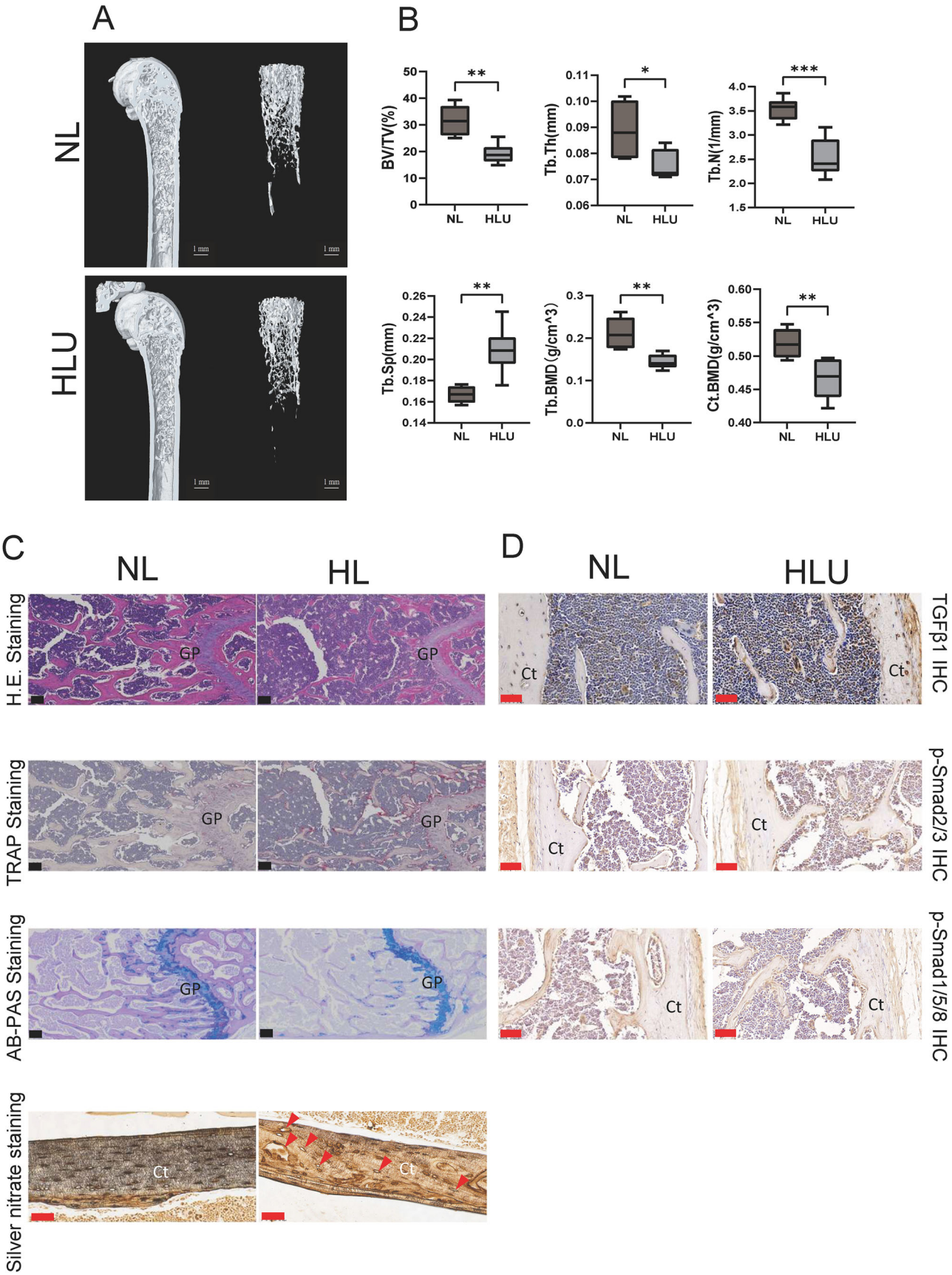
A
NL
HLU
1 mm
B
BV/TV(%)
Tb.Th(mm)
Tb.N(1/mm)
Tb.Sp(mm)
Tb.BMD (g/cm^3)
Ct.BMD(g/cm^3)
NL
HLU
C
NL
HL
H.E. Staining
TRAP Staining
AB-PAS Staining
Silver nitrate staining
GP
Ct
D
NL
HLU
TGFβ1 IHC
p-Smad2/3 IHC
p-Smad1/5/8 IHC
Ct

Fig. 1 | Establishment of a mouse disuse osteoporosis model using the HLU/Tail-suspension method. A Micro-CT reconstruction image. **B** Micro-CT analysis ($n = 6$). **C** Morphology of distal femoral bone tissue, H.E. staining, TRAP staining, AB-PAS staining and silver nitrate staining. GP Growth Plate. **D** Cortical bone and bone marrow TGFβ1 immunohistochemistry, p-Smad2/3 immunohistochemistry, and p-Smad1/5/8 immunohistochemistry. Scale bar: Black/Red 50 μm. $^{*}p < 0.05$, $^{**}p < 0.01$, $^{***}p < 0.001$.

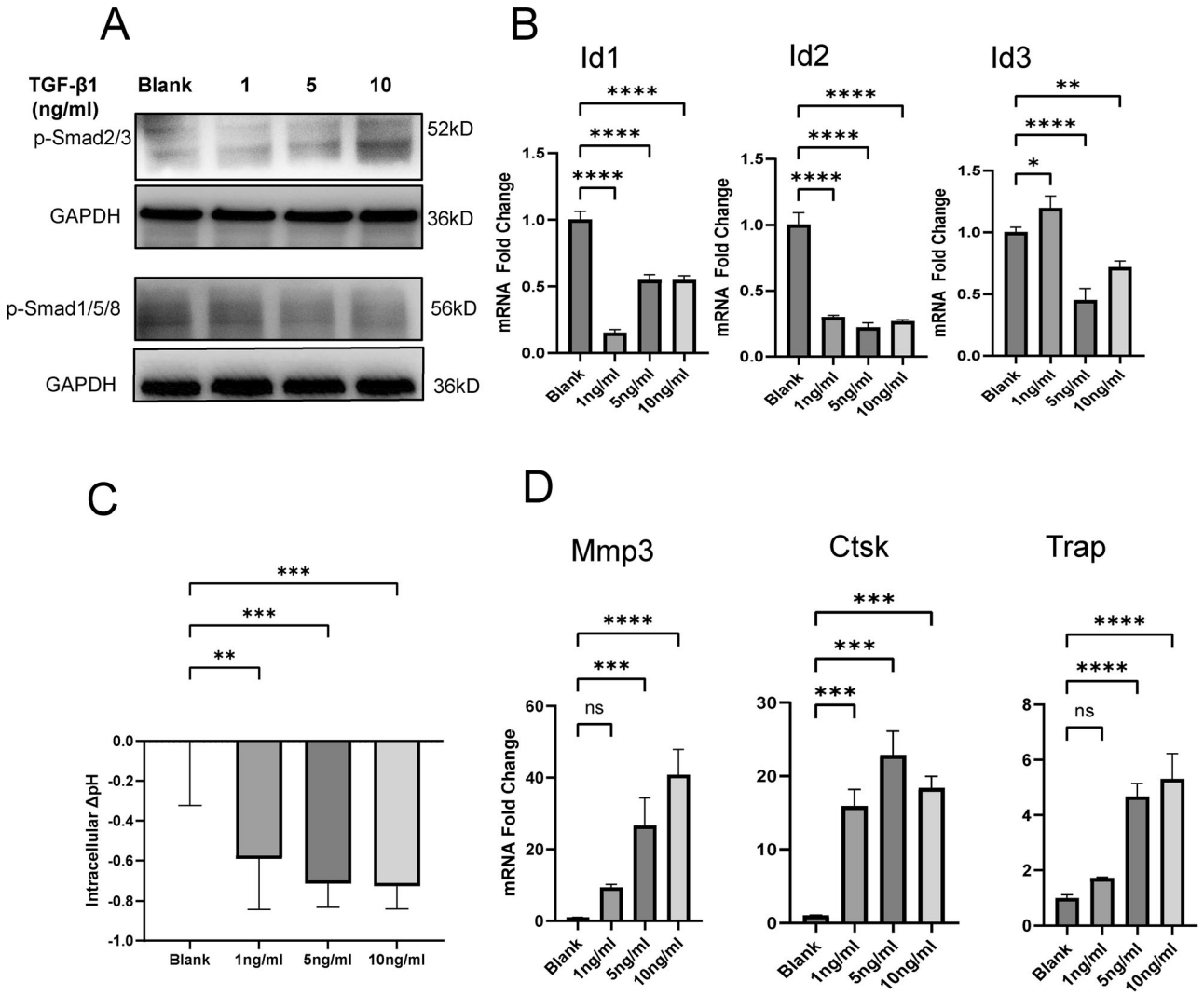

Fig. 2 | In vitro treatment of primary osteocytes with high concentrations of TGFβ1. A Western blot analysis of phosphorylated Smads in primary osteocytes stimulated with a high dose of TGFβ1 for 3 days. **B** Expression of BMP-pSmad1/5/8 downstream target genes in primary osteocytes treated with varying concentrations of TGFβ1 for 3 days. **C** Intracellular pH changes in response to different concentrations of TGFβ1. **D** Expression of osteolytic factors in primary osteocytes induced by different concentrations of TGFβ1. $^{*}p < 0.05$, $^{**}p < 0.01$, $^{***}p < 0.001$, $^{****}p < 0.0001$.

suspension unloading (Fig. 7A). The Tb.BMD and Ct.BMD in HLU+Adv-BMP9 mice were significantly higher than those in the HLU group injected with the control virus (Fig. 7B). Bone microstructural parameters such as BV/TV, trabecular thickness (Tb.Th) and trabecular number (Tb.N) demonstrated that in vivo adenoviral overexpression of BMP9 effectively improved disuse osteoporosis in the femur induced by HLU/Tail-suspension (Fig. 7B). Additionally, a biomechanical testing device was used to examine the effect of Adv-BMP9 on bone mechanical properties. HLU mice exhibited significant declines in femoral stiffness and elastic modulus (>30% decrease; Fig. 7C). Adv-BMP9 treatment restored these biomechanical parameters to control levels, demonstrating BMP9's ability to mitigate the adverse effects of unloading on bone mechanics (Fig. 7C). Serological testing data demonstrate that adenovirus vector muscle injection can increase the BMP9 levels in mouse serum (Supplementary Fig. 2B).

Histological Images and immunohistochemistry show that Adv-BMP9 (GDF2) improves bone microstructural degradation induced by HLU

H.E. staining results showed that in the control virus group, the trabecular bone morphology in HLU mice was severely degraded, while injection of Adv-BMP9 effectively improved the trabecular bone morphology (Fig. 8A). TRAP staining results showed that injection of Adv-BMP9 in the HLU group significantly inhibited the TRAP-positive cells induced by HLU. Interestingly, we observed a strong effect of BMP9 on the growth plate. In the group injected with the control virus, as mentioned in previous modeling results, the primary trabecular bone generated by the growth plate in the HLU group was severely atrophied, whereas in the Adv-BMP9-injected mice, the development of the growth plate was protected. The observed reduction in empty lacunae following BMP9 intervention, as evidenced by

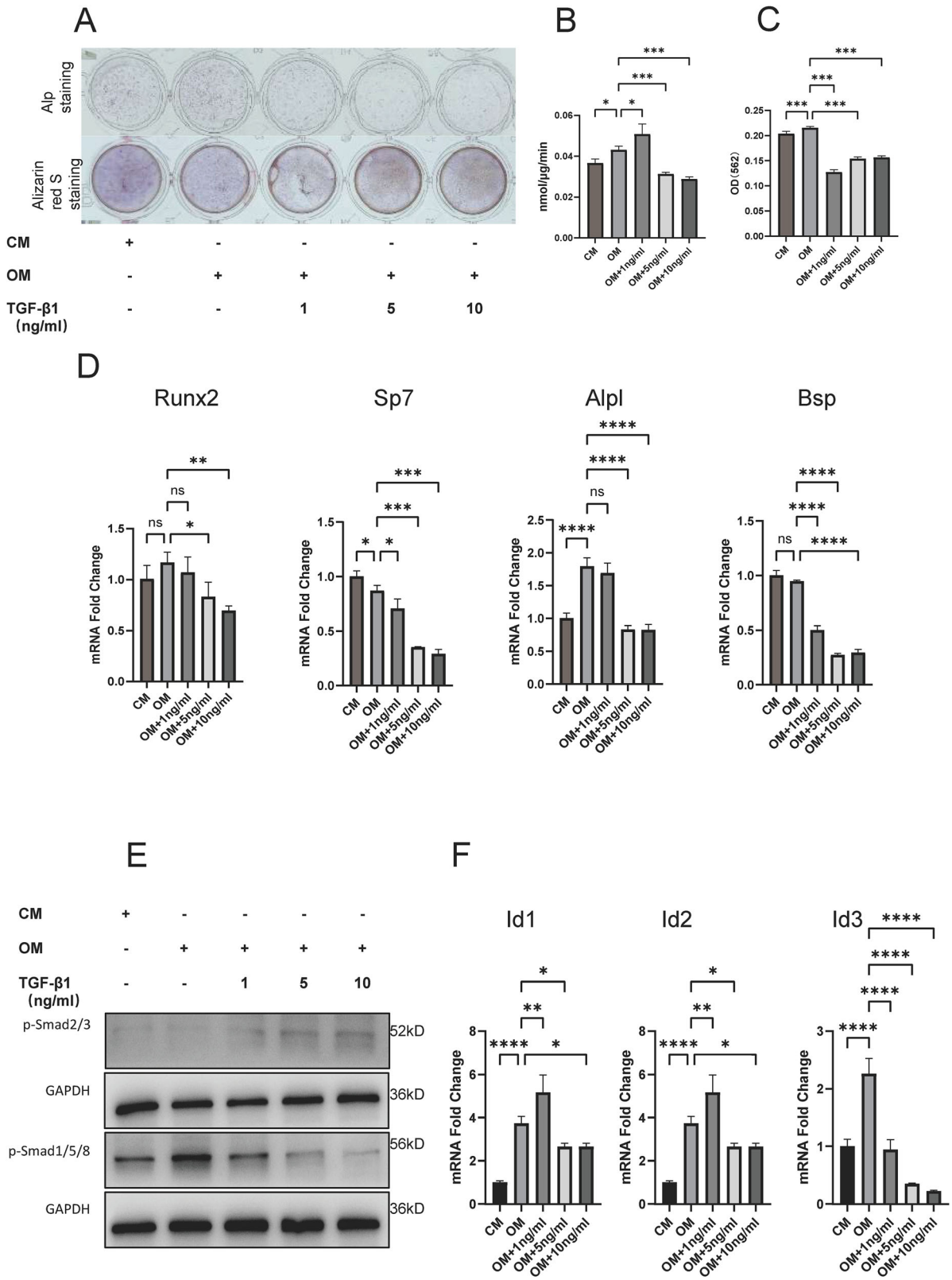

Fig. 3 | High concentration of TGFβ1 inhibits osteogenic differentiation of marrow stromal cells in vitro. A Alkaline phosphatase staining and Alizarin Red S staining. **B** Alkaline phosphatase enzyme activity. **C** Quantification of mineralization. **D** Osteogenic gene expression ($n = 3$). **E** Phosphorylation of Smads following high-dose TGFβ1 treatment in vitro, as detected by western blot. **F** Alteration of BMP-pSmad1/5/8 signaling target genes in marrow stromal cells by high-dose TGFβ1 in vitro ($n = 3$). CM Control culture medium, OM=Osteogenic induction medium. ns no significance $^{*}p < 0.05$, $^{**}p < 0.01$, $^{***}p < 0.001$, $^{****}p < 0.0001$.

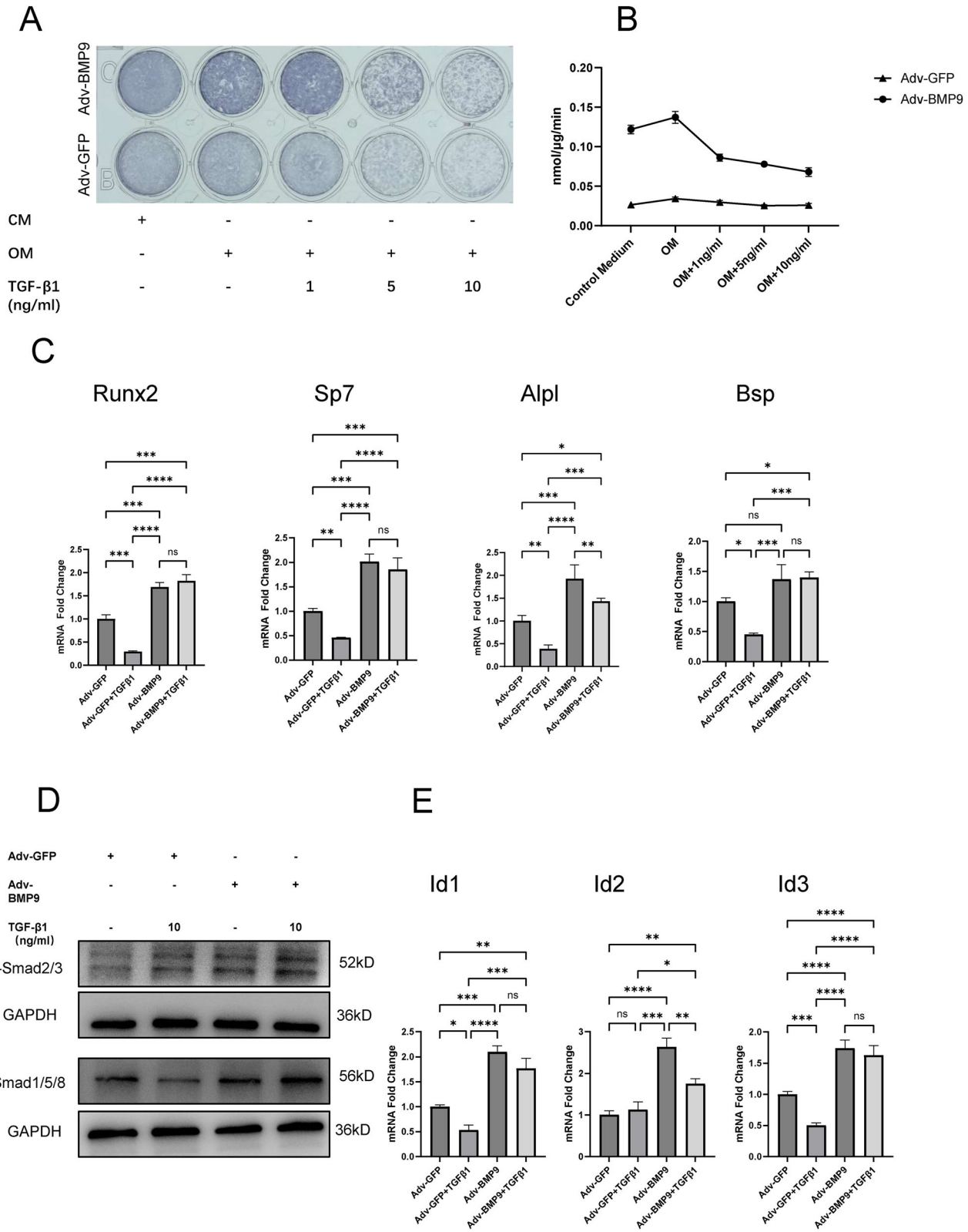

Fig. 4 | Adv-BMP9 infection in marrow stromal cells alleviates osteogenic inhibition induced by high concentration of TGFβ1. A Alkaline phosphatase staining. **B** Quantification of alkaline phosphatase enzyme activity. **C** Osteogenic gene expression following infection with Adv-BMP9 or control virus in the presence of 10 ng/ml TGFβ1 ($n = 3$). **D** Phosphorylation of Smads in marrow stromal cells following infection with Adv-BMP9 or control virus in the presence of 10 ng/ml TGFβ1, as detected by western blot. **E** BMP-pSmad1/5/8 signaling target gene expression in marrow stromal cells following infection with Adv-BMP9 or control virus in the presence of 10 ng/ml TGFβ1 ($n = 3$). ns no significance, $^{*}p < 0.05$, $^{**}p < 0.01$, $^{***}p < 0.001$, $^{****}p < 0.0001$.

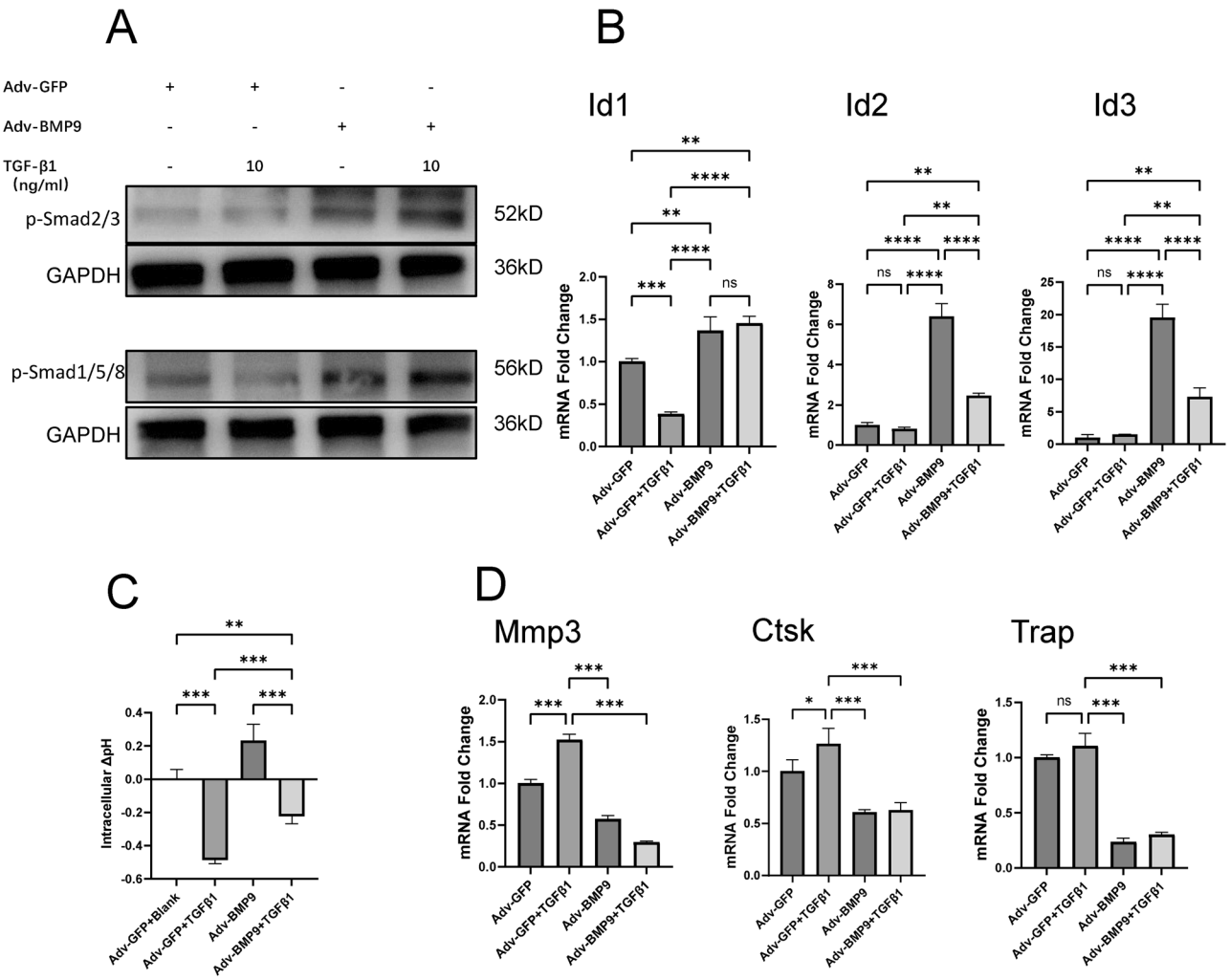

Fig. 5 | Adv-BMP9 infection of primary osteocytes alleviates the osteocytic transcriptional phenotype and cell acidification induced by high concentrations of TGFβ1. A Phosphorylation of Smads in primary osteocytes following infection with Adv-BMP9 or control virus in the presence of 10 ng/ml TGFβ1, as detected by western blot. **B** BMP-pSmad1/5/8 signaling target gene expression in primary osteocytes following infection with Adv-BMP9 or control virus in the presence of 10 ng/ml TGFβ1 ($n = 3$). **C** Intracellular pH changes in primary osteocytes following infection with Adv-BMP9 or control virus in the presence of 10 ng/ml TGFβ1, normalized to control group. **D** Expression of osteoclastic genes in primary osteocytes following infection with Adv-BMP9 or control virus in the presence of 10 ng/ml TGFβ1 ($n = 3$). ns no significance, $^{*}p < 0.05$, $^{**}p < 0.01$, $^{***}p < 0.001$, $^{****}p < 0.0001$.

silver nitrate staining, partially elucidates the mechanism underlying the preservation of cortical bone density (Fig. 8B). Immunohistochemical results showed that in Adv-BMP9-injected mice, there were more p-Smad1/5/8-positive cells in both cortical bone and the marrow cavity, indicating that muscle injection of Adv-BMP9 can upregulate BMP-pSmad1/5/8 signaling in bone tissue for bone protection.

Discussion

Disuse osteoporosis, as a unique form of secondary osteoporosis, is directly caused by the loss of mechanical stress, leading to an imbalance in bone metabolism[32]. Following the disruption of the balance between bone formation and resorption (i.e., bone metabolic imbalance), deterioration of the bone microarchitecture is accompanied by increased skeletal fragility. This significantly elevates the risk of fractures in specific scenarios, such as during re-entry into gravitational field by astronauts or rehabilitation exercises in long-term bedridden patients[33,34]. Although previous studies have highlighted the critical roles of pathways such as Wnt/β-catenin and the RANKL/OPG axis[35–39], and proposed drug intervention strategies like bisphosphonates and sclerostin antibodies[40–43], there is still a lack of systematic research on the precise regulation of TGFβ/BMP signaling imbalance in the context of disuse osteoporosis. This is particularly true for strategies aimed at restoring bone metabolic homeostasis under conditions such as microgravity or prolonged immobilization. In this study, we employed the tail-suspension method to construct a hindlimb unloading (HLU) mouse model, in combination with an in vitro simulated microgravity environment. We systematically revealed that TGFβ/BMP signaling imbalance may play a crucial role in the cellular dynamics and molecular mechanisms underlying the development of disuse osteoporosis. Additionally, for the first time, we applied an adenoviral overexpression of BMP9 (GDF2) as a therapeutic strategy to restore bone metabolic homeostasis in the HLU model.

Through the construction of a disuse osteoporosis mouse model and Micro-CT analysis of femoral samples, this study found that mice exhibited significant bone loss after 14 days of hindlimb unloading: trabecular bone density (Tb.BMD) decreased over 30%, cortical bone density (Ct.BMD) reduced over 10%, bone volume fraction (BV/TV), trabecular number (Tb.N), and trabecular thickness (Tb.Th) all significantly decreased. These phenotypes are similar to the bone loss observed in patients with disuse osteoporosis, such as astronauts who lose an average of 1–1.5% of bone mineral density (BMD) per month[15,44]. Taking into account the age-conversion relationship between rodents and humans[45], as well as the BMD changes observed in our experiments,

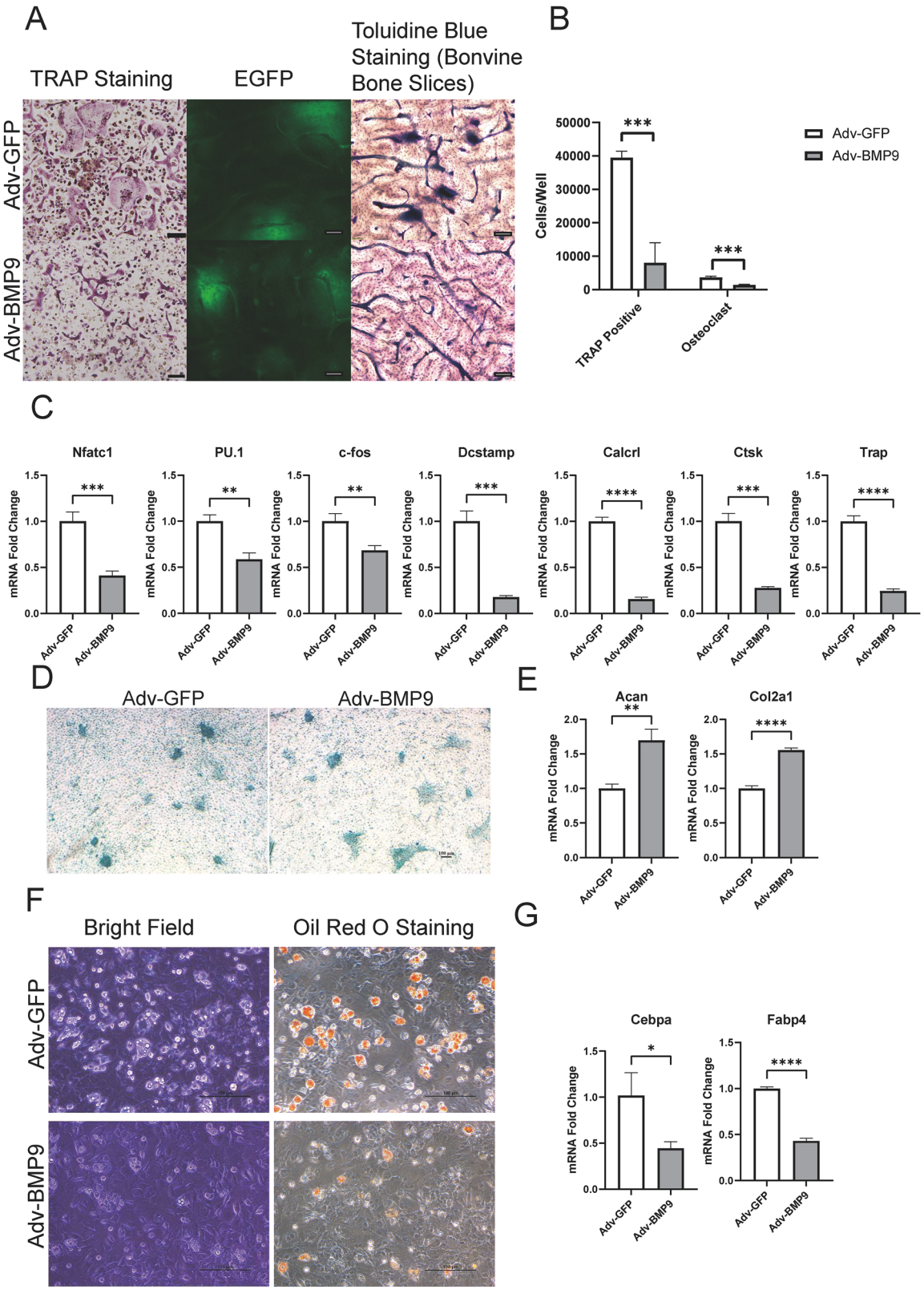

Fig. 6 | Adv-BMP9 inhibits osteoclastogenesis, suppresses adipogenic differentiation of marrow stromal cells, and promotes chondrogenic differentiation. **A** Osteoclastogenesis assay: TRAP staining and bovine bone slice osteoclast resorption assay, Scale bar: Black/White 50 μm. **B** TRAP-positive cell count and osteoclast count ($n = 3$). **C** Osteoclastogenesis gene expression analysis ($n = 3$). **D** Alizarin Blue staining for chondrogenic differentiation of marrow stromal cells after 7 days of induction. **E** Chondrogenic differentiation gene expression in marrow stromal cells ($n = 3$). **F** Adipogenic differentiation assay: bright field/ Oil Red O staining of marrow stromal cells after 7 days of induction. **G** Adipogenic differentiation-related gene expression in marrow stromal cells ($n = 3$). $^{*}p < 0.05$, $^{**}p < 0.01$, $^{***}p < 0.001$, $^{****}p < 0.0001$.

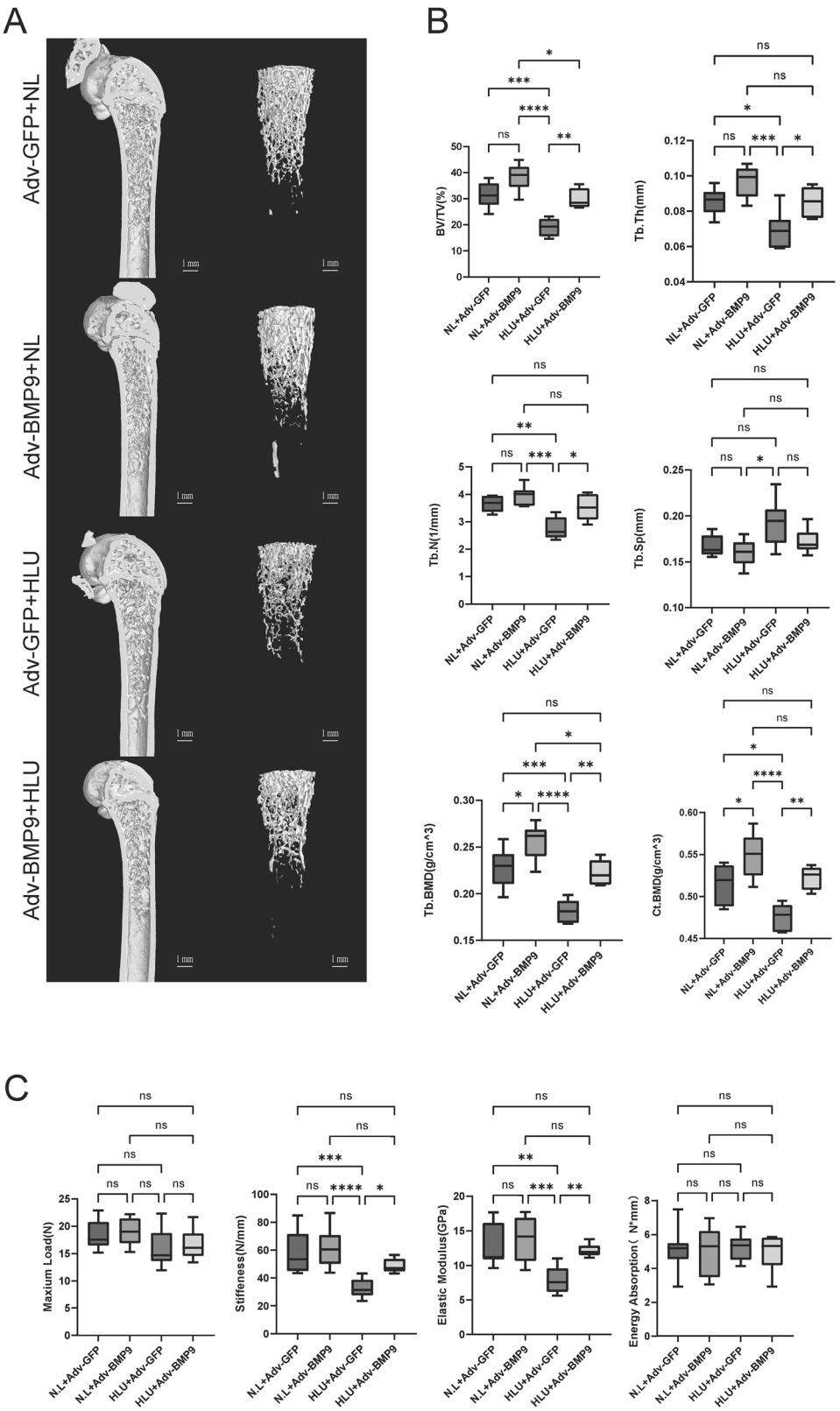

Fig. 7 | Intramuscular injection of Adv-BMP9 improves bone loss induced by HLU/Tail-Suspension and enhances femoral mechanical properties. A Micro-CT reconstruction images. **B** Micro-CT analysis data ($n = 6$). **C** Three-point bending test data ($n = 6$). ns=no significance, $^{*}p < 0.05$, $^{**}p < 0.01$, $^{***}p < 0.001$, $^{****}p < 0.0001$.

we estimate that two weeks of tail suspension in rodents may simulate a period of extreme skeletal unloading in humans equivalent to over one year, potentially approaching two years. Further histological analysis revealed trabecular bone structure degradation (H.E. staining), restricted growth plate cartilage development (AB-PAS staining), disrupted lacunar canalicular systems (silver nitrate staining), and significantly enhanced osteoclast activity as shown by TRAP staining in the HLU group. These results suggest that disuse osteoporosis is not merely a static manifestation of bone loss, but rather involves a disruption of the dynamic balance between bone formation and resorption, orchestrated by multiple cell types within the bone microstructure. Immunohistochemical results further showed that the levels of phosphorylated Smad2/3 (downstream

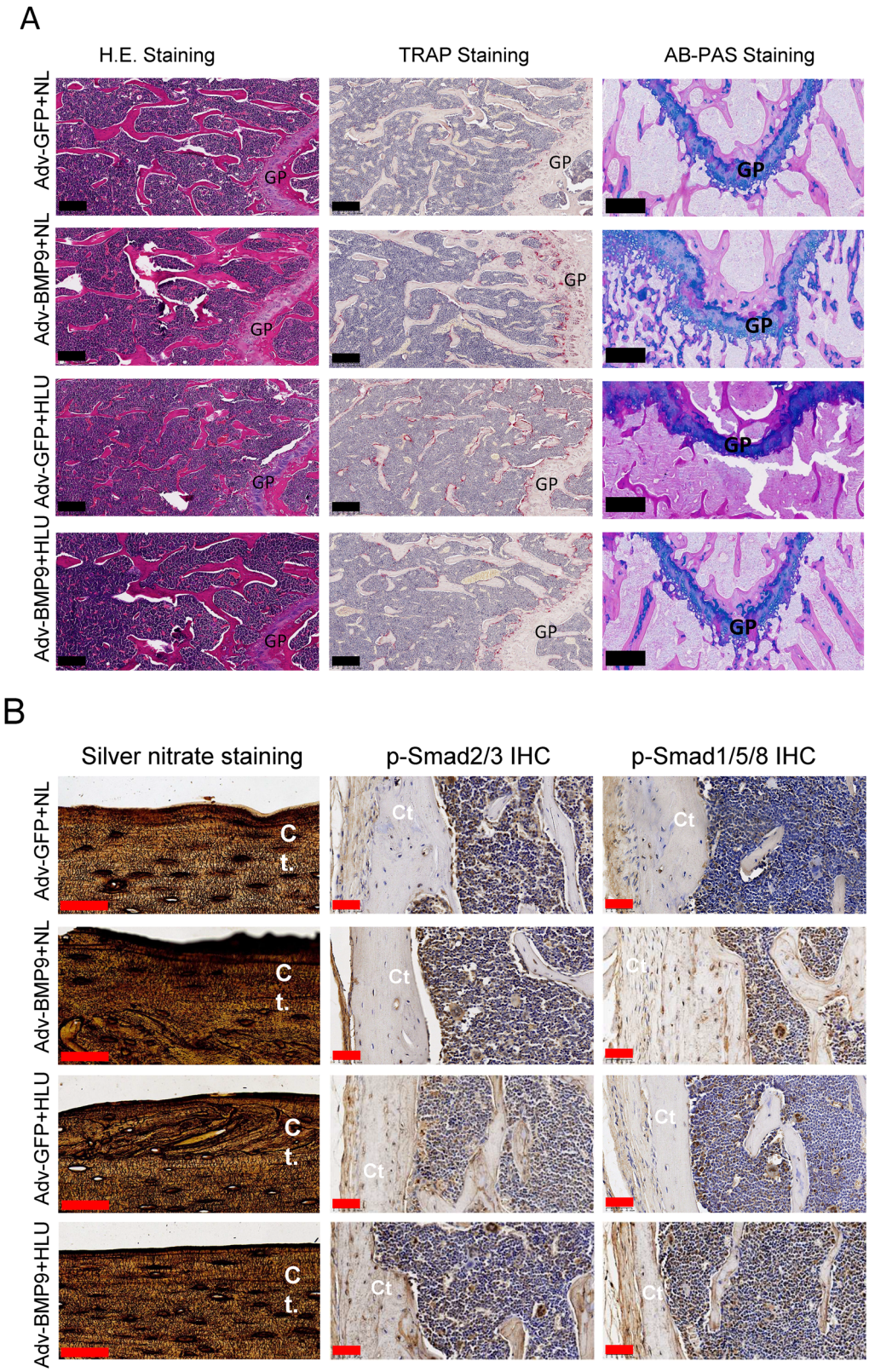

Fig. 8 | Intramuscular injection of Adv-BMP9 improves bone tissue morphological changes induced by HLU/Tail-Suspension. A H.E. staining, TRAP staining, and AB-PAS staining. **B** Silver nitrate staining, p-Smad2/3 immunohistochemistry, and p-Smad1/5/8 immunohistochemistry. Scale bar: Black 200 μm; Red 50 μm.

effectors of TGFβ signaling) were significantly elevated in the bone tissue of the HLU group mice, while phosphorylated Smad1/5/8 (downstream effectors of BMP signaling) were inhibited. For the first time, we report this "TGFβ signaling enhancement - BMP signaling suppression" imbalance pattern in a disuse osteoporosis model and propose that it may disrupt the osteoblast-osteoclast balance through intracellular and extracellular competitive mechanisms, such as the occupation of common transcriptional cofactors like Smad4[46]. The core scientific question raised by these findings is: Does the imbalance in TGFβ/BMP signaling drive disuse osteoporosis?

The combination of a rotating cell culture system and 3D integrated printing approach also suggests that osteocytes may participate in osteolysis under microgravity conditions. According to the modeling results of a simple differential equation system, the shear stress exerted on the biomimetic module in the RCCS container exceeds 1.6 Pa (approximately 16 dynes/cm²), which surpasses the threshold that can induce osteoblast differentiation[47,48]. Due to the limited precision of the printer, the module's size could not avoid the effects of shear stress. As a result, it was challenging to construct a biomimetic module to simulate osteoblast inhibition caused by microgravity. Based on the calculations, we speculate that to simulate a low shear stress environment, the cell carrier size must be controlled at the micron level (Supplementary Discussion). In future experiments, the preparation of microsphere-based cell carriers may be a necessary choice[49]. Thus, in our in vitro experiments, we are more inclined to focus on the role of cellular TGFβ/BMP signaling balance in osteoblasts and osteocytes.

During the osteogenic induction of bone marrow stromal cells, 10 ng/mL of TGFβ1 significantly decreased the expression and enzyme activity of alkaline phosphatase, reduced the expression of osteogenic genes (*Runx2*, *Sp7*, *Alpl*, and *Bsp*), and inhibited mineralization. As osteocytes are the most abundant resident cell type in the bone matrix, their dysfunction may play a critical role in disuse osteoporosis. This study found that 10 ng/mL of TGFβ1 significantly increased the expression of osteolytic factors *Mmp3*, *Ctsk*, and *Trap* in osteocytes, while also lowering intracellular pH. This suggests that disuse may lead to an acidified microenvironment in osteocytes, promoting bone matrix degradation, which aligns closely with osteocytic observed in pathological conditions[50]. This finding extends the traditional "osteoclast-centered" view of bone resorption[51,52] and emphasizes the active role of osteocytes in osteolysis during disuse osteoporosis[53–55]. Western blot analysis of both BMSCs and osteocytes showed increased levels of p-Smad2/3 in the TGFβ1-treated group, while p-Smad1/5/8 levels were decreased, confirming the antagonistic competition between these two signaling pathways. Interestingly, both TGFβ-pSmad2/3 and BMP-pSmad1/5/8 have been reported as key signaling pathways for the differentiation of stem cells into osteoblasts[28]. TGFβ signaling is considered a critical pathway guiding early migration, differentiation, and lineage commitment of mesenchymal stem cells through a concentration gradient-dependent mechanism[56,57], while BMP signaling is indispensable in the process of mesenchymal stem cell differentiation into osteoblasts[58,59]. Although some reports indicate that high local concentrations of TGFβ1 impair osteogenic differentiation, thereby affecting bone defect repair[60], the role of TGFβ signaling in osteoporosis remains controversial[23,61]. Our experimental results appear to uncouple the functional roles of TGFβ and BMP signaling in the osteogenic lineage, emphasizing their competitive relationship. While the exact mechanisms underlying this competition remain to be determined, prior research indicates potential involvement of competition for receptor phosphorylation sites[46,62] or restriction of nuclear translocation of transcriptional complexes like Smad4-CoSmad[63,64]. Furthermore, multi-tiered inhibitory mechanisms are plausible, as evidenced by reports that TGFβ1 suppresses BMP2 expression through Tmeff1, thereby inhibiting BMP signaling and influencing mesenchymal stem cell osteogenic differentiation[65]. Additionally, we observed increased marrow adiposity, characterized by round or oval voids, which aligns with established findings in disuse osteoporosis[66,67]. This prompts consideration of whether endogenous BMP inhibitors derived from marrow fat might disrupt the equilibrium between TGFβ and BMP signaling[68–70].

Although the specific competitive mechanism was not explored, based on experimental observations and the previously raised scientific questions, we considered restoring BMP-pSmad1/5/8 signaling as a potential strategy to counteract bone loss in the HLU model. Among the many BMP family members, BMP9 (GDF2) has emerged as an ideal osteogenic factor due to its potent osteogenic activity and resistance to antagonistic properties[29,30]. Our experiments using an adenoviral vector to overexpress BMP9 successfully restored the expression and enzymatic activity of alkaline phosphatase in bone marrow stromal cells in vitro, as well as rescued the osteogenic gene expression suppressed by TGFβ1. For osteocytes, Adv-BMP9 was able to restore intracellular pH and limit the expression of osteolytic factors. Additionally, BMP9 exhibits pleiotropic regulatory functions, such as inhibiting adipogenesis and promoting chondrogenesis, while simultaneously suppressing osteoclastogenesis. These findings correlate with in vivo results, where Adv-BMP9 treatment significantly improved bone density, trabecular parameters, and mechanical properties, and partially restored the lacunar canalicular system. Furthermore, growth plate cartilage development was fully supported under Adv-BMP9 treatment. Despite no decrease in p-Smad2/3 levels, the increased proportion of p-Smad1/5/8 positive cells in bone tissue from the BMP9 treatment group further suggests a "signal balance" mechanism.

Our animal studies confirm BMP9's function in mitigating bone loss during disuse. However, the fixed injection and modeling schedules limit our ability to exclude the peak bone mass hypothesis as a confounding factor[71]. This hypothesis suggests that pre-disuse BMP9 administration may enhance femoral bone mass, potentially accounting for the observed differences in bone loss between groups. Future studies could address this by varying the sequence of treatments. Central to our investigation is the dynamic interplay between TGFβ and BMP signaling pathways in the molecular pathogenesis of disuse osteoporosis. Guided by the 'TGFβ/BMP signaling balance hypothesis' and informed by the dysregulation of osteoblast-osteoclast equilibrium and chondrocyte development observed in our model, we selected BMP9 as a therapeutic intervention. Compared to currently widely used osteoporosis drugs such as alendronate, denosumab, or calcitriol[72–75], BMP9 possesses multiple actions that confer significant advantages—primarily, its dual functionality in promoting osteogenesis while inhibiting osteoclastogenesis, a feature unmatched by monotherapeutic agents that either stimulate bone formation (e.g., PTH derivatives) or suppress bone resorption. Additionally, BMP9's stimulatory effect on chondrogenesis could be pivotal for long bone matrix remodeling, despite the limited attention given to cartilage developmental restrictions under disuse conditions. Finally, given the emerging evidence implicating osteocytes as central players in disuse osteoporosis, our comprehensive data reveal that BMP9-mediated regulation of osteocyte function is sufficient to influence bone matrix remodeling.

However, translating BMP9 into clinical application will not be an easy task, not only because it has been reported to be associated with ectopic ossification or myositis ossificans[76,77], but also due to the limited clinical use of BMP ligands. To date, only rhBMP2 and rhBMP7 have been approved by the FDA[78,79], specifically for spinal fusion and craniofacial bone repair. This is largely due to concerns about the safety and cost of using BMP ligands[80]. Regarding safety, our data suggest a potential solution: developing a gene therapy strategy specifically targeting osteocytes. Essentially, our experimental design is based on an adenoviral vector-mediated gene delivery system. Given the concerns regarding the safety and stability of adenoviral vectors[81,82], strategies that specifically target bone tissue—or even osteocytes—are worth pursuing. For example, adeno-associated viruses (AAVs) modified through capsid engineering to incorporate short Asp-Ser-Ser (DSS) peptide sequences may enhance vector affinity for the bone matrix[83,84]. In combination with the osteocyte-specific promoter DMP1[85–87], BMP9 expression could be restricted to osteocytes, thereby limiting its effects to bone tissue. Whether this approach can effectively minimize potential side effects from the vector or the therapeutic factor itself remains to be confirmed through further experimental investigation. As for cost, current anti-osteoporotic drugs such as denosumab are associated with a rebound in bone resorption upon discontinuation[88,89]. This necessitates either concurrent administration of bisphosphonates like alendronate or prolonged treatment, which undermines both temporal and economic efficiency[90]. If a stable adeno-associated virus expression vector can be developed, its expression duration could support a single-dose intervention lasting over a year[91–93]. This offers a clear cost advantage compared to denosumab, which requires administration every six months—or even more frequently[94].

This study is the first to focus on the dynamic balance between TGFβ and BMP signaling in the molecular mechanisms underlying disuse osteoporosis. By adopting a multi-faceted and multi-modal approach, we

explored the competitive inhibitory relationship between TGFβ-pSmad2/3 and BMP-pSmad1/5/8, providing new insights into the regulation of bone metabolism. Although the RCCS system, which simulates a microgravity environment, has limitations—such as shear stress interference that prevents a full replication of osteoblast suppression—our method successfully induced increased expression of osteocyte-derived *Sost* and osteolytic factors, thereby laying the groundwork for a deeper understanding of osteocyte function. To address the system's limitations, we proposed targeted improvements based on computational modeling, specifically by reducing carrier density and size (Supplementary Discussion). Finally, both in vitro and in vivo experiments demonstrated the bone-protective role of BMP9 under disuse conditions, offering a potential therapeutic strategy for osteoporosis, particularly disuse-induced osteoporosis.

Methods

Construction of adenoviral overexpression vectors using the Admax system

The packaging plasmid pBHGlox(delta)E13Cre and shuttle plasmid pDC316-mCMV-EGFP-CMV-mGdf2/pDC316-mCMV-EGFP were purchased from Baoxian Laboratory (Baoxian Laboratory, China). The packaging and shuttle plasmids were co-transfected into the 293 A cell line using PEI transfection reagent (MCE, New Jersey, USA) to induce recombination via the Cre-loxp system. After 14 days of culture, floating cells and supernatant were collected, and the primary viruses Adv-GFP and Adv-BMP9 were obtained using a freeze-thaw cycle method[95]. After three rounds of repeated infection of the 293 A cell line, a high-titer viral suspension was obtained. The titer was then determined using the Spearman-Karber method. The adenoviral vector concentration and purification were performed using cesium chloride ultracentrifugation and dialysis to obtain a viral concentrate with a titer of 1×10^10 pfu/mL, which was then used for cell or animal experiments[96,97].

Extraction and culture of primary bone marrow stromal cells and osteocytes

After euthanizing the mice and obtaining the femurs, the bone marrow cavities were rinsed with sterile phosphate-buffered saline (PBS, Biosharp, China).After cutting off the epiphyses, the bone marrow was flushed out using sterile phosphate-buffered saline (PBS, Biosharp, China). After centrifugation at 200xg, the bone marrow was resuspended in complete α-MEM medium (Gibco, USA) containing 10% FBS (Shanghai Sangon, China) and 1% penicillin-streptomycin (Solarbio, China). The cells were then seeded into a 10 cm cell culture dish. After one week, the cells were passaged and used for subsequent trilineage differentiation experiments. Primary osteocytes were obtained by alternately treating bone fragments with 5 mM EDTA.2Na (Chongqing Chuandong Chemical, China) solution and 0.1% (w/v) type I collagenase(Sigma-Aldrich, USA), followed by culturing the fragments[98–101].

Trilineage differentiation of bone marrow stromal cells and TGFβ1 intervention

For osteogenic differentiation of bone marrow stromal cells, osteogenic induction medium (OM) was prepared by adding 0.1 μM dexamethasone, 10 mM β-glycerophosphate disodium salt, and 50 mg/mL vitamin C to the complete medium[102]. After infecting the bone marrow stromal cells with Adv-EGFP/BMP9 at an MOI of 200, the cells were seeded onto 24-well or 6-well cell culture plates, followed by the addition of osteogenic induction medium or complete medium, with different concentrations of TGFβ1 (0, 1, 5, 10 ng/mL) for intervention. After 1-7 days of culture, samples were collected for alkaline phosphatase staining (Beyotime Biotech, China) and relevant molecular assays, following the manufacturer's protocol. For chondrogenic differentiation, after infection with Adv-BMP9 or Adv-EGFP, TGFβ3 (10 ng/mL, Topscience, China) was added to F12/DMEM 1:1 (Gibco, USA) containing 10% fetal bovine serum (Shanghai Sangon, China) and 1% penicillin-streptomycin (Solarbio, China). Additionally, 0.1 μM dexamethasone, 50 μg/mL vitamin C, and 1% ITS (Beyotime Biotech, China) were used for 7 days of induction, followed by Alcian Blue staining (Beyotime Biotech, China) and molecular assays[103]. For adipogenic differentiation, following the infection with the adenoviral vector, 1 μM dexamethasone was added to DMEM (Gibco, USA) containing 10% fetal bovine serum (Shanghai Sangon, China) and 1% penicillin-streptomycin (Solarbio, China). Additionally, 0.5 mM IBMX, 100 μM indomethacin, and 10 μg/mL recombinant human insulin (Beyotime Biotech, China) were used for 7 days of induction, followed by Oil Red O staining and relevant molecular assays[104].

BMMs culture, osteoclast induction, and TRAP staining

Bone marrow cells from the femur and tibia were flushed with DMEM, then cultured in DMEM containing 10% FBS and 100 ng/mL macrophage colony-stimulating factor (M-CSF; Topscience, China) for 24 h. The floating cells in the supernatant were collected and cultured in DMEM containing 10% FBS (Shanghai Sangon, China), 1% penicillin-streptomycin mixture, and 30 ng/mL M-CSF for 3 days to generate BMMs. During this period, the cells were infected with Adv-GFP or Adv-BMP9 at an MOI of 400. To generate mature osteoclasts, the cells were induced for osteoclast differentiation in α-MEM containing 10% FBS (Shanghai Sangon, China), 50 ng/mL RANKL (RANKL; Topscience, China), and 30 ng/mL M-CSF (Topscience, China) for 4-7 days[71,105,106]. According to the manufacturer's protocol, the cells were stained for tartrate-resistant acid phosphatase (TRAP) using a macrophage acid phosphatase kit (Sigma-Aldrich, USA). TRAP-positive multinucleated cells with more than three nuclei were considered osteoclasts. Osteoclasts were observed, photographed, and quantified under a microscope.

Construction of cell/GelMA hydrogel/PCL biomimetic functional modules and microgravity simulation

GelMA (SunP Biotech, Beijing, China) was completely dissolved in α-MEM medium to prepare a 20% (w/v) solution, which was then filtered through a 0.22 μm filter. MC3T3-E1, ATDC5, MLO-Y4, or BMSCs were trypsinized and resuspended in basic culture medium. After mixing with GelMA, the photoinitiator (LAP) (SunP Biotech, Beijing, China) was added. The final concentrations of the passaged cell lines, GelMA, and LAP were 10^6 cells/mL, 10% (v/v), and 0.25% (v/v), respectively. PCL (SunP Biotech, Beijing, China) was sterilized by UV irradiation for 1 h before use. The rigid biomaterial and cell-integrated 3D system was designed by the Bone Development and Regeneration Laboratory at Chongqing Medical University, based on previous research[107–110]. The spiral nozzle containing the PCL material and the bio-ink cartridge containing the passaged cell lines were computer-controlled and moved along the X, Y, and Z axes. Before printing, the PCL was placed into a molten spiral extrusion nozzle and melted at 95 °C for 10 min. Meanwhile, the GelMA solution containing the cell lines was placed into a syringe, after which the syringe was placed into the pneumatic extrusion nozzle for subsequent printing. The melted PCL was then printed to form columns with a width of 300 μm. GelMA hydrogel loaded with cells was then printed between the PCL strips, with a spacing of 400 μm between cell clusters. Each printed layer was irradiated with 405 nm blue light for 5 s to stabilize and solidify. After printing, the scaffold was immersed in sterile PBS for 1 min and repeated 3 times to remove excess LAP photoinitiator. After 3 days of culture in the corresponding induction medium, the modules was used for RCCS simulated microgravity cell experiments. The rotating cell culture system (RCCS) for microgravity was developed in collaboration between NASA and MIT at the end of the last century. It uses the principle of equivalence to apply centrifugal force in a non-inertial frame of reference to balance gravity and create a simulated microgravity environment[110]. The Cell/GelMA hydrogel/PCL biomimetic functional module prepared in the previous step was placed into the rotating cell culture system(RCCS, Suzhou Qianyun Instruments Co., Ltd., China, ESCO). Following the manufacturer's instructions, the culture containers were sterilized before use. The module was cut to an appropriate size to fit the container, and the system was placed into a cell culture incubator at 37 °C with 5% CO_2 for the experiment. The RCCS rotational speed was adjusted to 28-35 rpm to

ensure that the biomimetic modules suspended in the center of the container for suspended culture to simulate microgravity. After seven days, samples were collected for related molecular analysis.

Reverse transcription real-time fluorescent quantitative PCR detection

Total RNA was extracted using the AG RNAex Pro kit (Accurate Biology, China), and then reverse transcribed into cDNA using the Evo M-MLV reverse transcription kit (Accurate Biology, China) for real-time fluorescent quantitative PCR detection. Real-time quantitative PCR (qPCR) was performed using the SYBR Green Pro Taq HS premixed qPCR kit (Accurate Biology, China) on the Gentier 96E system (Tianlong Science and Technology, Xi'an, China).The relative mRNA expression levels were normalized to the housekeeping gene *Gapdh* using the 2(-Delta Delta C(T)) method, and expression changes were quantified[111–113]. The primer list is Supplementary Table 1.

Establishment of the mouse disuse osteoporosis model and adenovirus vector in vivo experiment

NASA and the University of California School of Medicine established a classic model to simulate the occurrence of disuse osteoporosis in long bones under microgravity conditions, known as the Hindlimbs Unloading (HLU)/Tail-suspension method[113–116]. This model simulates the physiological response of long bones to the absence of axial stress on Earth. Fourteen-week-old male C57BL/6 J mice, with similar body weights, were purchased from the Experimental Animal Center of Chongqing Medical University (Chongqing, China). The mice were divided into Hindlimbs Unloading (HLU) and Normal Load (NL) groups for model establishment. In each group, mice were injected with either Adv-GFP or Adv-BMP9 purified viruses via intramuscular injection (10^9 pfu per mouse) in the hindlimb thigh muscles. Four experimental groups were created: HLU+Adv-GFP, HLU+Adv-BMP9, NL +Adv-GFP, and NL+Adv-BMP9. The HLU group mice were housed individually in tail-suspension cages. The tail was suspended using medical tape and cotton string, with the tail attached to a metal rack in the cage. The environmental temperature was maintained at 22 °C ± 1 °C, with a 12-h dark/12-h light cycle. The duration of the HLU experiment was 14 days, which, according to the rodent-to-human age conversion, is equivalent to approximately two years of unloading in humans[45]. Although the activity of the HLU group mice was restricted, they had unrestricted access to standard rodent food and water. The mice were anesthetized with isoflurane (2% inhalation until fully anesthetized), followed by collection of 500 µL whole blood via tail vein for serological analysis. The mice were then euthanized using CO_2 at a flow rate of 10 L/min for 10 min. The study protocol was approved by the Institutional Animal Care and Use Committee (IACUC) of Chongqing Medical University.

Adenovirus overexpression of BMP9 in bone marrow stromal cells and osteocytes in vitro

Due to the abnormal activation of p-Smad2/3 signaling observed in the HLU model, and the inability of RCCS combined with 3D-integrated printing to adequately simulate the osteogenesis inhibition caused by microgravity, the in vitro simulated microgravity model will no longer be used. We found that the highly activated TGFβ-pSmad2/3 signaling pathway can inhibit osteogenic differentiation in bone marrow stromal cells. Bone marrow stromal cells were extracted using the previously mentioned method[105], infected with Adv-BMP9 or control virus, and then treated with osteogenic induction medium (OM) containing TGFβ1 at concentrations of 1, 5, and 10 ng/mL (Topscience, China) to assess its impact on osteogenic function. For osteocytes, the corresponding concentrations of TGFβ1 were also added to investigate the molecular-level changes. Intracellular pH changes in osteocytes were evaluated using the Prynine probe (Topscience, China)[117].

Micro-CT analysis

The left femur of each mouse was isolated, and as much soft tissue as possible was removed. The femora were then fixed overnight in 4% neutral paraformaldehyde (Biosharp, China) before undergoing Micro-CT scanning (XuanZun Bio, Chongqing, China). Bone and MAT scans were performed using the Bruker Micro-CT Skyscan 1276 system (Kontich, Belgium). Scan parameters were as follows: tube current 200 µA, voltage 70 kV, scanning the entire object with a resolution of 6.5µm, exposure time of 350 ms, and a scanning angle of 180 degrees. Phantom scans (provided by the equipment manufacturer for calibration) were performed under the same conditions. A total of 2300 layers were scanned and reconstructed using NRecon software (Version 1.7.4.2). The reconstruction was then analyzed using CTAn (Version 1.20.3.0). Starting from the distal femoral growth plate, manual segmentation of trabecular and cortical bone was performed on each scanned slice, and the cortical and trabecular bone regions were subsequently analyzed separately.[118]. The following parameters were analyzed: trabecular bone density (Tb.BMD, g/cm^3), trabecular volume percentage (BV/TV, %), trabecular thickness (Tb.Th, mm), trabecular number (Tb.N, 1/mm), and cortical bone density (Ct.BMD, g/cm^3) ($n = 6$).

Histology and immunohistochemistry

After euthanizing, the femur was obtained, and all non-bone tissues were removed as thoroughly as possible. The femur was then fixed overnight in 4% paraformaldehyde (Biosharp, China) and decalcified for 14 days in sterile 14% ethylenediaminetetraacetic acid disodium salt (EDTA.2Na) at pH 7.4. After decalcification, the femur was paraffin-embedded and sectioned at 5 µm thickness. Longitudinal coronal sections of the femur were prepared. The sections were stained with hematoxylin and eosin (H.E.) (Servicebio, China). Osteoclasts were histologically stained using the TRAP staining kit (Servicebio, China)[119]. Alcian Blue/Periodic Acid-Schiff (AB-PAS) staining (AB-PAS staining solution, Servicebio, China) was used to observe the development of growth plate cartilage[120]. For immunohistochemistry, the decalcified femur was paraffin-embedded and sectioned at 5 µm. Standard three-step avidin-biotin complex immunohistochemical staining was performed[121]. The primary antibodies used were anti-TGF beta 1 (1:200 dilution, Affinity, China), anti-p-Smad2/3 (1:200 dilution, Affinity, China) and anti-p-Smad1/5/8 (1:200 dilution, Affinity, China).

Western blot

For western blot, total protein lysates were obtained by mixing RIPA buffer (Beyotime Biotech, China) with protease/phosphatase inhibitors (Beyotime Biotech, China). After denaturation, the protein lysates were subjected to SDS-PAGE and transferred onto a PVDF membrane (Millipore, Burlington, MA, USA). The membrane was then blocked with 5% non-fat milk (Beyotime Biotech, China) at room temperature for 1 h and incubated overnight at 4 °C with primary antibodies against p-Smad2/3 and p-Smad1/5/8 (1:1000 dilution, Affinity, China). The enzyme-conjugated secondary antibody was incubated at room temperature for 1 h.

Three-point bending test

After fixation of femur with 4% paraformaldehyde, The femur was fixed at two points 7 mm apart, and the load sensor advanced at a rate of 2 mm per minute until the bone fractured. The three-point bending test was conducted using a mechanical testing machine (CellScale, USA) on the femurs[122,123]. During the bending test, the computer data acquisition system collected load-displacement data at a sampling rate of 100 Hz. Biomechanical data were custom-calculated, including maximum load (N), stiffness (N/mm), elastic modulus (Pa), and energy absorption (N*mm). The elastic modulus was approximated using cortical bone data (Ct.Ar and Tt.Ar) from Micro-CT, calculating the moment of inertia and generating the elastic modulus from stiffness data[124].

Serum elisa analysis and alkaline phosphatase activity quantification

A terminal blood collection method was used, where mice were anesthetized with isoflurane, followed by collection of 500 µl of blood via the facial vein. The blood was then centrifuged at 3000 rpm at 4 °C for 15 min. Serum levels of PINP, CTX-I, and BMP9 were measured using ELISA (Jiangsu Meimian industrial, MM-43891M2, MM-43816M2 and MM-48164M2 China) according to the manufacturer's instructions. For cell samples, protein lysates were obtained using IP-grade cell lysis buffer (Beyotime Biotech, China), and the protein concentration was measured using a BCA protein assay kit (Beyotime Biotech, China). Alkaline phosphatase activity in the samples was assessed using an alkaline phosphatase assay kit (Beyotime Biotech, China). Unit enzyme activity was calculated using the data from both assays to evaluate the osteogenic potential of mesenchymal stem cells[125].

Statistical methods

Experimental data were analyzed statistically using GraphPad Prism 10.1.2. Comparison between two independent samples was performed using a t-test, while comparison among multiple samples with a single factor was done using one-way ANOVA. For comparison among multiple factors, two-way ANOVA was applied. A p-value of less than 0.05 was considered statistically significant.

Data availability

All data and codes generated for this study are available from the corresponding authors upon reasonable request.

Received: 13 March 2025; Accepted: 18 July 2025;
Published online: 01 August 2025

References

1. Sözen, T., Özışık, L. & Başaran, N. Ç An overview and management of osteoporosis. *Eur. J. Rheumatol.* **4**, 46–56 (2017).
2. Lane, J. M., Russell, L. & Khan, S. N. Osteoporosis. *Clin. Orthop. Relat. Res* **372**, 139–150 (2000).
3. Rashki Kemmak, A. et al. Economic burden of osteoporosis in the world: A systematic review. *Med J. Islam Repub. Iran.* **34**, 154 (2020).
4. Shen, Y. et al. The Global Burden of Osteoporosis, Low Bone Mass, and Its Related Fracture in 204 Countries and Territories, 1990-2019. *Front Endocrinol.* **13**, 882241 (2022).
5. Frenk, J. et al. Health professionals for a new century: transforming education to strengthen health systems in an interdependent world. *Lancet* **376**, 1923–1958 (2010).
6. Gao, S. et al. Current scenario and challenges of clinical pharmacists to implement pharmaceutical care in DRG/DIP payment hospitals in China: a qualitative interview study. *Front Public Health* **12**, 1339504 (2024).
7. Cox-York, K. A., Erickson, C. B., Pereira, R. I., Bessesen, D. H. & Van Pelt, R. E. Region-specific effects of oestradiol on adipose-derived stem cell differentiation in post-menopausal women. *J. Cell Mol. Med* **21**, 677–684 (2017).
8. Fu, Y. et al. Adipogenic differentiation potential of adipose-derived mesenchymal stem cells from ovariectomized mice. *Cell Prolif.* **47**, 604–614 (2014).
9. Stubbins, R. E., Najjar, K., Holcomb, V. B., Hong, J. & Núñez, N. P. Oestrogen alters adipocyte biology and protects female mice from adipocyte inflammation and insulin resistance. *Diabetes Obes. Metab.* **14**, 58–66 (2012).
10. Moerman, E. J., Teng, K., Lipschitz, D. A. & Lecka-Czernik, B. Aging activates adipogenic and suppresses osteogenic programs in mesenchymal marrow stroma/stem cells: the role of PPAR-gamma2 transcription factor and TGF-beta/BMP signaling pathways. *Aging Cell* **3**, 379–389 (2004).
11. Li, Y. et al. Nicotinamide phosphoribosyltransferase (Nampt) affects the lineage fate determination of mesenchymal stem cells: a possible cause for reduced osteogenesis and increased adipogenesis in older individuals. *J. Bone Min. Res* **26**, 2656–2664 (2011).
12. Yeung, D. K. W. et al. Osteoporosis is associated with increased marrow fat content and decreased marrow fat unsaturation: a proton MR spectroscopy study. *J. Magn. Reson Imaging* **22**, 279–285 (2005).
13. Kim, J. H. & Kim, N. Bone Cell Communication Factors Provide a New Therapeutic Strategy for Osteoporosis. *Chonnam Med J.* **56**, 94–98 (2020).
14. Pignolo, R. J., Law, S. F. & Chandra, A. Bone aging, cellular senescence, and osteoporosis. *JBMR* **5**, e10488 (2021).
15. Rolvien, T. & Amling, M. Disuse Osteoporosis: Clinical and Mechanistic Insights. *Calcif. Tissue Int* **110**, 592–604 (2022).
16. Whedon, G. D. Disuse osteoporosis: physiological aspects. *Calcif. Tissue Int* **36**, S146–S150 (1984).
17. Rittweger, J. et al. Bone loss in the lower leg during 35 days of bed rest is predominantly from the cortical compartment. *Bone* **44**, 612–618 (2009).
18. Garrett-Bakelman, F. E. et al. The NASA Twins Study: A multidimensional analysis of a year-long human spaceflight. *Science* **364**, eaau8650 (2019).
19. Juhl, O. J. et al. Update on the effects of microgravity on the musculoskeletal system. *NPJ Microgravity* **7**, 28 (2021).
20. Edwards, W. B., Schnitzer, T. J. & Troy, K. L. Bone mineral loss at the proximal femur in acute spinal cord injury. *Osteoporos. Int* **24**, 2461–2469 (2013).
21. Buettmann, E. G. et al. Similarities Between Disuse and Age-Induced Bone Loss. *J. Bone Min. Res* **37**, 1417–1434 (2022).
22. MacFarlane, E. G., Haupt, J., Dietz, H. C. & Shore, E. M. TGF-β Family Signaling in Connective Tissue and Skeletal Diseases. *Cold Spring Harb. Perspect. Biol.* **9**, a022269 (2017).
23. van Zoelen, E. J., Duarte, I., Hendriks, J. M. & van der Woning, S. P. TGFβ-induced switch from adipogenic to osteogenic differentiation of human mesenchymal stem cells: identification of drug targets for prevention of fat cell differentiation. *Stem Cell Res Ther.* **7**, 123 (2016).
24. Quinn, J. M. et al. Transforming growth factor beta affects osteoclast differentiation via direct and indirect actions. *J. Bone Min. Res* **16**, 1787–1794 (2001).
25. Dole, N. S. et al. Osteocyte-Intrinsic TGF-β Signaling Regulates Bone Quality through Perilacunar/Canalicular Remodeling. *Cell Rep.* **21**, 2585–2596 (2017).
26. Balooch, G. et al. TGF-beta regulates the mechanical properties and composition of bone matrix. *Proc. Natl Acad. Sci. USA* **102**, 18813–18818 (2005).
27. Lowery, J. W. & Rosen, V. The BMP Pathway and Its Inhibitors in the Skeleton. *Physiol. Rev.* **98**, 2431–2452 (2018).
28. Chen, G., Deng, C. & Li, Y. P. TGF-β and BMP signaling in osteoblast differentiation and bone formation. *Int J. Biol. Sci.* **8**, 272–288 (2012).
29. Cheng, H. et al. Osteogenic activity of the fourteen types of human bone morphogenetic proteins (BMPs). *J. Bone Jt. Surg. Am.* **85**, 1544–1552 (2003).
30. Song, T., Huang, D. & Song, D. The potential regulatory role of BMP9 in inflammatory responses. *Genes Dis.* **9**, 1566–1578 (2022).
31. Kang, Q. et al. Characterization of the distinct orthotopic bone-forming activity of 14 BMPs using recombinant adenovirus-mediated gene delivery. *Gene Ther.* **11**, 1312–1320 (2004).
32. Grygorieva, N. V., Dedukh, N. V., Parubets, M. M. & Bystrytska, M. A. Disuse (post-mobilization) osteoporosis: literature review and clinical case series. *PJS* **12**, 94–107 (2022).

33. Gabel, L. et al. Incomplete recovery of bone strength and trabecular microarchitecture at the distal tibia 1 year after return from long duration spaceflight. *Sci. Rep.* **12**, 9446 (2022).
34. Axpe, E. et al. A human mission to Mars: Predicting the bone mineral density loss of astronauts. *PLoS One* **15**, e0226434 (2020).
35. Robling, A. G. et al. Mechanical stimulation of bone in vivo reduces osteocyte expression of Sost/sclerostin. *J. Biol. Chem.* **283**, 5866–5875 (2008).
36. Gioia, M. et al. Simulated microgravity induces a cellular regression of the mature phenotype in human primary osteoblasts. *Cell Death Discov.* **4**, 59 (2018).
37. Mann, V. et al. Changes in Human Foetal Osteoblasts Exposed to the Random Positioning Machine and Bone Construct Tissue Engineering. *Int J. Mol. Sci.* **20**, 1357 (2019).
38. Rucci, N., Rufo, A., Alamanou, M. & Teti, A. Modeled microgravity stimulates osteoclastogenesis and bone resorption by increasing osteoblast RANKL/OPG ratio. *J. Cell Biochem* **100**, 464–473 (2007).
39. Kawao, N., Morita, H., Iemura, S., Ishida, M. & Kaji, H. Roles of Dkk2 in the Linkage from Muscle to Bone during Mechanical Unloading in Mice. *Int J. Mol. Sci.* **21**, 2547 (2020).
40. Galea, G. L., Lanyon, L. E. & Price, J. S. Sclerostin's role in bone's adaptive response to mechanical loading. *Bone* **96**, 38–44 (2017).
41. Rosenthal, R., Schneider, V. S., Jones, J. A. & Sibonga, J. D. The Case for Bisphosphonate Use in Astronauts Flying Long-Duration Missions. *Cells* **13**, 1337 (2024).
42. Ha, P. et al. Bisphosphonate conjugation enhances the bone-specificity of NELL-1-based systemic therapy for spaceflight-induced bone loss in mice. *NPJ Microgravity* **9**, 75 (2023).
43. Brent, M. B., Brüel, A. & Thomsen, J. S. Anti-sclerostin antibodies and abaloparatide have additive effects when used as a countermeasure against disuse osteopenia in female rats. *Bone* **160**, 116417 (2022).
44. Lang, T. F., Leblanc, A. D., Evans, H. J. & Lu, Y. Adaptation of the proximal femur to skeletal reloading after long-duration spaceflight. *J. Bone Min. Res* **21**, 1224–1230 (2006).
45. Dutta, S. & Sengupta, P. Men and mice: Relating their ages. *Life Sci.* **152**, 244–248 (2016).
46. Martinez-Hackert, E., Sundan, A. & Holien, T. Receptor binding competition: A paradigm for regulating TGF-β family action. *Cytokine Growth Factor Rev.* **57**, 39–54 (2021).
47. Mai, Z. et al. Single Bout Short Duration Fluid Shear Stress Induces Osteogenic Differentiation of MC3T3-E1 Cells via Integrin β1 and BMP2 Signaling Cross-Talk. Shi X. M., ed. *PLoS ONE*. 2013;8:e61600.
48. Goodwin, T. J., Prewett, T. L., Wolf, D. A. & Spaulding, G. F. Reduced shear stress: A major component in the ability of mammalian tissues to form three-dimensional assemblies in simulated microgravity. *J. Cell. Biochem.* **51**, 301–311 (1993).
49. Mashiko, T. et al. Selective Proliferation of Highly Functional Adipose-Derived Stem Cells in Microgravity Culture with Stirred Microspheres. *Cells* **10**, 560 (2021).
50. Tsourdi, E., Jähn, K., Rauner, M., Busse, B. & Bonewald, L. F. Physiological and pathological osteocytic osteolysis. *J Musculoskelet Neuronal Interact* **18**, 292–303 (2018).
51. Charles, J. F. & Aliprantis, A. O. Osteoclasts: more than "bone eaters. *Trends Mol. Med* **20**, 449–459 (2014).
52. Boyle, W. J., Simonet, W. S. & Lacey, D. L. Osteoclast differentiation and activation. *Nature* **423**, 337–342 (2003).
53. Bonewald, L. F. & Johnson, M. L. Osteocytes, mechanosensing and Wnt signaling. *Bone* **42**, 606–615 (2008).
54. Blaber, E. A. et al. Microgravity Induces Pelvic Bone Loss through Osteoclastic Activity, Osteocytic Osteolysis, and Osteoblastic Cell Cycle Inhibition by CDKN1a/p21. Vanacker J. M., ed. *PLoS ONE*. 2013;8:e61372.
55. Cabahug-Zuckerman, P. et al. Osteocyte Apoptosis Caused by Hindlimb Unloading is Required to Trigger Osteocyte RANKL Production and Subsequent Resorption of Cortical and Trabecular Bone in Mice Femurs. *J. Bone Miner. Res.* **31**, 1356–1365 (2016).
56. Tang, Y. et al. TGF-beta1-induced migration of bone mesenchymal stem cells couples bone resorption with formation. *Nat. Med* **15**, 757–765 (2009).
57. Itoh, F., Watabe, T. & Miyazono, K. Roles of TGF-β family signals in the fate determination of pluripotent stem cells. *Semin Cell Dev. Biol.* **32**, 98–106 (2014).
58. Shi, C. et al. Deletion of BMP receptor type IB decreased bone mass in association with compromised osteoblastic differentiation of bone marrow mesenchymal progenitors. *Sci. Rep.* **6**, 24256 (2016).
59. Valcourt, U. & Moustakas, A. BMP Signaling in Osteogenesis, Bone Remodeling and Repair. *Eur. J. Trauma* **31**, 464–479 (2005).
60. Xu, J. et al. High-Dose TGF-β1 Impairs Mesenchymal Stem Cell-Mediated Bone Regeneration via Bmp2 Inhibition. *J. Bone Min. Res* **35**, 167–180 (2020).
61. Erlebacher, A. & Derynck, R. Increased expression of TGF-beta 2 in osteoblasts results in an osteoporosis-like phenotype. *J. Cell Biol.* **132**, 195–210 (1996).
62. Wu, M., Wu, S., Chen, W. & Li, Y. P. The roles and regulatory mechanisms of TGF-β and BMP signaling in bone and cartilage development, homeostasis and disease. *Cell Res* **34**, 101–123 (2024).
63. Dituri, F., Cossu, C., Mancarella, S. & Giannelli, G. The Interactivity between TGFβ and BMP Signaling in Organogenesis, Fibrosis, and Cancer. *Cells* **8**, 1130 (2019).
64. Yuan, G., Zhan, Y., Gou, X., Chen, Y. & Yang, G. TGF-β signaling inhibits canonical BMP signaling pathway during palate development. *Cell Tissue Res* **371**, 283–291 (2018).
65. Xu, J. et al. High-Dose TGF-β1 Impairs Mesenchymal Stem Cell–Mediated Bone Regeneration via Bmp2 Inhibition. *J. Bone Min. Res* **35**, 167–180 (2020).
66. Buettmann, E. G. et al. Similarities Between Disuse and Age-Induced Bone Loss. *J. Bone Miner. Res.* **37**, 1417–1434 (2022).
67. Trudel, G. et al. Bone marrow fat accumulation after 60 days of bed rest persisted 1 year after activities were resumed along with hemopoietic stimulation: the Women International Space Simulation for Exploration study. *J. Appl Physiol. (1985)* **107**, 540–548 (2009).
68. Zou, W. et al. Ablation of Fat Cells in Adult Mice Induces Massive Bone Gain. *Cell Metab.* **32**, 801–813.e6 (2020).
69. Canalis, E., Economides, A. N. & Gazzerro, E. Bone morphogenetic proteins, their antagonists, and the skeleton. *Endocr. Rev.* **24**, 218–235 (2003).
70. Sawant, A. et al. Noggin is novel inducer of mesenchymal stem cell adipogenesis: implications for bone health and obesity. *J. Biol. Chem.* **287**, 12241–12249 (2012).
71. Li, A. et al. Pharmacologic Calcitriol Inhibits Osteoclast Lineage Commitment via the BMP-Smad1 and IκB-NF-κB Pathways. *J. Bone Min. Res* **32**, 1406–1420 (2017).
72. Pavone, V. et al. Pharmacological Therapy of Osteoporosis: A Systematic Current Review of Literature. *Front Pharm.* **8**, 803 (2017).
73. Siris, E. Alendronate in the treatment of osteoporosis: a review of the clinical trials. *J. Women's Health Gend. Based Med* **9**, 599–606 (2000).
74. Silva-Fernández, L., Rosario, M. P., Martínez-López, J. A., Carmona, L. & Loza, E. Denosumab for the treatment of osteoporosis: a systematic literature review. *Reumatol. Clin.* **9**, 42–52 (2013).
75. Tilyard, M. W., Spears, G. F., Thomson, J. & Dovey, S. Treatment of postmenopausal osteoporosis with calcitriol or calcium. *N. Engl. J. Med* **326**, 357–362 (1992).
76. Zhao, C. et al. BMP-9 mediates fibroproliferation in fibrodysplasia ossificans progressiva through TGF-β signaling. *EMBO Mol. Med* **17**, 112–128 (2025).

77. Leblanc, E. et al. BMP-9-induced muscle heterotopic ossification requires changes to the skeletal muscle microenvironment. *J. Bone Min. Res* **26**, 1166–1177 (2011).
78. On, S. W. et al. Current Status of Recombinant Human Bone Morphogenetic Protein-2 (rhBMP-2) in Maxillofacial Surgery: Should It Be Continued?. *Bioeng. (Basel)* **10**, 1005 (2023).
79. Ekrol, I., Hajducka, C., Court-Brown, C. & McQueen, M. M. A comparison of RhBMP-7 (OP-1) and autogenous graft for metaphyseal defects after osteotomy of the distal radius. *Injury* **39**, S73–S82 (2008).
80. Virk, S., Sandhu, H. S. & Khan, S. N. Cost effectiveness analysis of graft options in spinal fusion surgery using a Markov model. *J. Spinal Disord. Tech.* **25**, E204–E210 (2012).
81. Wang, Z. & Zhang, X. Adenovirus vector-attributed hepatotoxicity blocks clinical application in gene therapy. *Cytotherapy* **23**, 1045–1052 (2021).
82. Christ, M. et al. Modulation of the inflammatory properties and hepatotoxicity of recombinant adenovirus vectors by the viral E4 gene products. *Hum. Gene Ther.* **11**, 415–427 (2000).
83. Yarbrough, D. K. et al. Specific Binding and Mineralization of Calcified Surfaces by Small Peptides. *Calcif. Tissue Int* **86**, 58–66 (2010).
84. Yang, Y. S. et al. Bone-targeting AAV-mediated silencing of Schnurri-3 prevents bone loss in osteoporosis. *Nat. Commun.* **10**, 2958 (2019).
85. Lu, Y. et al. DMP1-targeted Cre expression in odontoblasts and osteocytes. *J. Dent. Res* **86**, 320–325 (2007).
86. Kalajzic, I. et al. Dentin matrix protein 1 expression during osteoblastic differentiation, generation of an osteocyte GFP-transgene. *Bone* **35**, 74–82 (2004).
87. Pang, J. L., Wu, B. L., Zhang, Y. Q., Zhao, H. P. & Liu, Y. L. Comparison and analysis of human dentin matrix protein 1 promoter activity in three different cells. *Hua Xi Kou Qiang Yi Xue Za Zhi* **24**, 148–152 (2006).
88. Anastasilakis, A. D. et al. Denosumab Discontinuation and the Rebound Phenomenon: A Narrative Review. *J. Clin. Med* **10**, 152 (2021).
89. Kim, A. S., Girgis, C. M. & McDonald, M. M. Osteoclast Recycling and the Rebound Phenomenon Following Denosumab Discontinuation. *Curr. Osteoporos. Rep.* **20**, 505–515 (2022).
90. Tsourdi, E. et al. Fracture risk and management of discontinuation of denosumab therapy: a systematic review and position statement by ECTS. *J Clin Endocrinol Metab*. Published online October 26, 2020:dgaa756.
91. Brommel, C. M., Cooney, A. L. & Sinn, P. L. Adeno-Associated Virus-Based Gene Therapy for Lifelong Correction of Genetic Disease. *Hum. Gene Ther.* **31**, 985–995 (2020).
92. George, L. A. et al. Long-Term Follow-Up of the First in Human Intravascular Delivery of AAV for Gene Transfer: AAV2-hFIX16 for Severe Hemophilia B. *Mol. Ther.* **28**, 2073–2082 (2020).
93. Herzog, R. W. Encouraging and Unsettling Findings in Long-Term Follow-up of AAV Gene Transfer. *Mol. Ther.* **28**, 341–342 (2020).
94. Shoback, D. et al. Pharmacological Management of Osteoporosis in Postmenopausal Women: An Endocrine Society Guideline Update. *J. Clin. Endocrinol. Metab.* **105**, dgaa048 (2020).
95. Zhang, H., Wang, H., An, Y. & Chen, Z. Construction and application of adenoviral vectors. *Mol. Ther. Nucleic Acids* **34**, 102027 (2023).
96. Nasukawa, T. et al. Virus purification by CsCl density gradient using general centrifugation. *Arch. Virol.* **162**, 3523–3528 (2017).
97. Luo, J. et al. A protocol for rapid generation of recombinant adenoviruses using the AdEasy system. *Nat. Protoc.* **2**, 1236–1247 (2007).
98. van der Plas, A. & Nijweide, P. J. Isolation and purification of osteocytes. *J. Bone Min. Res* **7**, 389–396 (1992).
99. Stern, A. R. et al. Isolation and culture of primary osteocytes from the long bones of skeletally mature and aged mice. *Biotechniques* **52**, 361–373 (2012).
100. Gu, G., Nars, M., Hentunen, T. A., Metsikkö, K. & Väänänen, H. K. Isolated primary osteocytes express functional gap junctions in vitro. *Cell Tissue Res* **323**, 263–271 (2006).
101. Gooi, J. H., Chia, L. Y., Vrahnas, C. & Sims, N. A. Isolation, Purification, Generation, and Culture of Osteocytes. *Methods Mol. Biol.* **1914**, 39–51 (2019).
102. Langenbach, F. & Handschel, J. Effects of dexamethasone, ascorbic acid and β-glycerophosphate on the osteogenic differentiation of stem cells in vitro. *Stem Cell Res Ther.* **4**, 117 (2013).
103. Mueller, M. B. & Tuan, R. S. Functional characterization of hypertrophy in chondrogenesis of human mesenchymal stem cells. *Arthritis Rheum.* **58**, 1377–1388 (2008).
104. Chen, Q. et al. Fate decision of mesenchymal stem cells: adipocytes or osteoblasts?. *Cell Death Differ.* **23**, 1128–1139 (2016).
105. Chevalier, C. et al. Primary mouse osteoblast and osteoclast culturing and analysis. *STAR Protoc.* **2**, 100452 (2021).
106. Li, Y. et al. Specific RANK Cytoplasmic Motifs Drive Osteoclastogenesis. *J. Bone Min. Res* **34**, 1938–1951 (2019).
107. Kang, H. W. et al. A 3D bioprinting system to produce human-scale tissue constructs with structural integrity. *Nat. Biotechnol.* **34**, 312–319 (2016).
108. Liu, G. et al. Functionalized 3D-Printed ST2/Gelatin Methacryloyl/Polcaprolactone Scaffolds for Enhancing Bone Regeneration with Vascularization. *IJMS* **23**, 8347 (2022).
109. Liu, Y. et al. The Osteocyte Stimulated by Wnt Agonist SKL2001 Is a Safe Osteogenic Niche Improving Bioactivities in a Polycaprolactone and Cell Integrated 3D Module. *Cells* **11**, 831 (2022).
110. Hammond, T. G. & Hammond, J. M. Optimized suspension culture: the rotating-wall vessel. *Am. J. Physiol.-Ren. Physiol.* **281**, F12–F25 (2001).
111. Livak, K. J. & Schmittgen, T. D. Analysis of relative gene expression data using real-time quantitative PCR and the 2(-Delta Delta C(T)) Method. *Methods* **25**, 402–408 (2001).
112. Schmittgen, T. D. & Livak, K. J. Analyzing real-time PCR data by the comparative C(T) method. *Nat. Protoc.* **3**, 1101–1108 (2008).
113. Morey-Holton, E. R. & Globus, R. K. Hindlimb unloading of growing rats: a model for predicting skeletal changes during space flight. *Bone* **22**, 83S–88S (1998).
114. Morey-Holton, E. R. & Globus, R. K. Hindlimb unloading rodent model: technical aspects. *J. Appl Physiol. (1985)* **92**, 1367–1377 (2002).
115. Lloyd, S. A., Lewis, G. S., Zhang, Y., Paul, E. M. & Donahue, H. J. Connexin 43 deficiency attenuates loss of trabecular bone and prevents suppression of cortical bone formation during unloading. *J. Bone Min. Res* **27**, 2359–2372 (2012).
116. Lloyd, S. A., Loiselle, A. E., Zhang, Y. & Donahue, H. J. Connexin 43 deficiency desensitizes bone to the effects of mechanical unloading through modulation of both arms of bone remodeling. *Bone* **57**, 76–83 (2013).
117. Giuliano, K. A. & Gillies, R. J. Determination of intracellular pH of BALB/c-3T3 cells using the fluorescence of pyranine. *Anal. Biochem* **167**, 362–371 (1987).
118. Bouxsein, M. L. et al. Guidelines for assessment of bone microstructure in rodents using micro-computed tomography. *J. Bone Min. Res* **25**, 1468–1486 (2010).
119. Taylor, L. M., Tertinegg, I., Okuda, A. & Heersche, J. N. Expression of calcitonin receptors during osteoclast differentiation in mouse metatarsals. *J. Bone Min. Res* **4**, 751–758 (1989).

120. Li, W. et al. Bevacizumab tested for treatment of knee osteoarthritis via inhibition of synovial vascular hyperplasia in rabbits. *J. Orthop. Transl.* **19**, 38–46 (2019).
121. Dabbs D. J. *Diagnostic Immunohistochemistry*. 6th ed. Elsevier, Inc; 2021.
122. Deckard, C., Walker, A. & Hill, B. J. F. Using three-point bending to evaluate tibia bone strength in ovariectomized young mice. *J. Biol. Phys.* **43**, 139–148 (2017).
123. Xiao, H. et al. BMP9 exhibits dual and coupled roles in inducing osteogenic and angiogenic differentiation of mesenchymal stem cells. *Biosci. Rep.* **40**, BSR20201262 (2020).
124. Leppänen, O., Sievänen, H., Jokihaara, J., Pajamäki, I. & Järvinen, T. L. N. Three-point bending of rat femur in the mediolateral direction: introduction and validation of a novel biomechanical testing protocol. *J. Bone Min. Res* **21**, 1231–1237 (2006).
125. Sabokbar, A., Millett, P. J., Myer, B. & Rushton, N. A rapid, quantitative assay for measuring alkaline phosphatase activity in osteoblastic cells in vitro. *Bone Min.* **27**, 57–67 (1994).

Acknowledgements

This research was funded by the National Natural Science Foundation of China 82471909(XL.T.), Chongqing Natural Science Foundation -Innovation and Development Joint Fund CSTB2022NSCQ-LZX0048 (XL.T.) and -General Project CSTB2024NSCQ-MSX0145 (YJ.L.); Chongqing Municipal Special Program for Technological Innovation and Application Development —Key Project CSTB2022TIAD-KPX0172 (GH.S.); National funded Post-doctoral Researcher Program of China GZC20233350 (YJ.L.); Research Project Funded by the Affiliated Yongchuan Hospital of Chongqing Medical University YJSJ202137 (GH.S.) and YJJL2024006 (YJ.L.).

Author contributions

Contributor Roles Taxonomy (CRediT) Author HY.Z.: Writing—original draft, Writing—review and editing, Data curation, Formal analysis, Methodology, Validation, Visualization. MF.Y.: Writing—original draft, Writing—review & editing, Data curation, Formal analysis, Investigation, Methodology, Validation, Visualization. Y.J.L.: Writing—review & editing, Funding acquisition, Investigation. Tu.X.: Writing—review & editing, Funding acquisition, Supervision, Resources, Project administration, Conceptualization. GH.S.: Writing—review & editing, Funding acquisition, Supervision, Resources, Project administration, Conceptualization.

Competing interests

The authors declare no competing interests.

Additional information

Supplementary information The online version contains supplementary material available at https://doi.org/10.1038/s41526-025-00510-y.

Correspondence and requests for materials should be addressed to Xiaolin Tu or Gaohai Shao.